Supplement of Clim. Past, 20, 2499–2524, 2024
https://doi.org/10.5194/cp-20-2499-2024-supplement

Climate of the Past
Open Access
EGU

Supplement of

The comparative role of physical system processes in Hudson Strait ice stream cycling: a comprehensive model-based test of Heinrich event hypotheses

Kevin Hank and Lev Tarasov

Correspondence to: Kevin Hank (khank@mun.ca)

S1 Full model domain

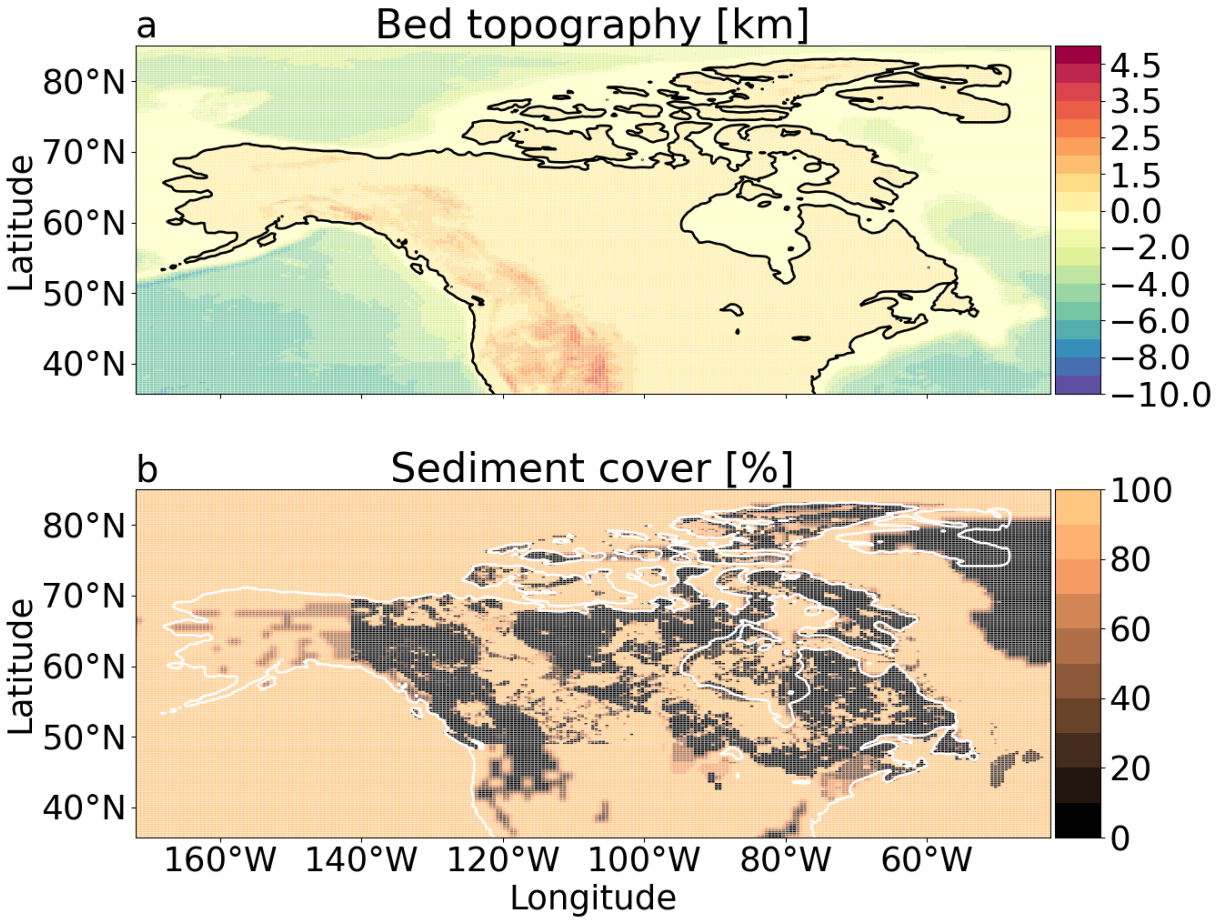

Figure S1. GSM input present-day bed topography and sediment cover for the full model domain. The black contour line shows the present-day sea level (coastline) used in the GSM. Note the change in the color bar step at 0 km in panel a.

S2 Maximum basal water thickness and grounding line treatment

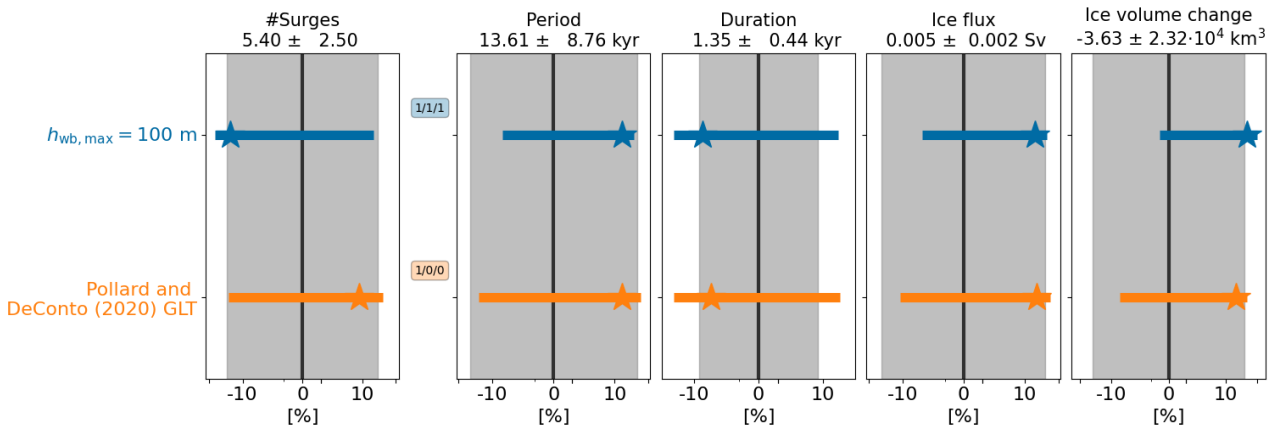

Figure S2. Percentage differences in surge characteristics compared to the reference setup. Only parameter vectors within the #surges > 2 sub-ensemble are considered. The model setups, from top to bottom, are $h_{\mathrm{wb,max}} = 100$ m and Pollard and Deconto (2020) grounding line treatment (GLT). Otherwise as Fig. 6

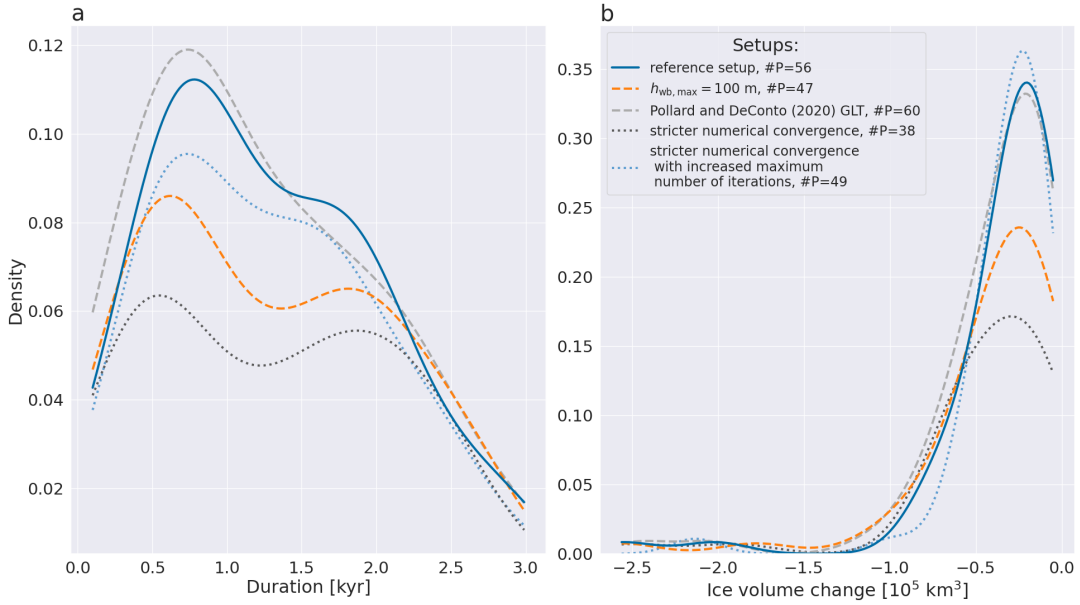

Figure S3. Kernel density plot for the whole ensemble (20 reference runs), a setup with increased maximum basal water thickness ($h_{\mathrm{wb,max}} = 100$ m), and a setup with a different grounding line treatment (GLT, Pollard and Deconto, 2020). The reference and MNEEs setups use the default $h_{\mathrm{wb,max}} = 10$ m and Schoof (2007) GLT. The $h_{\mathrm{wb,max}} = 100$ m and Pollard and Deconto (2020) GLT setups use the default Schoof (2007) GLT and $h_{\mathrm{wb,max}} = 10$ m, respectively. #P indicates the total number of surges across all runs of the ensemble.

S3 Input geothermal heat flux

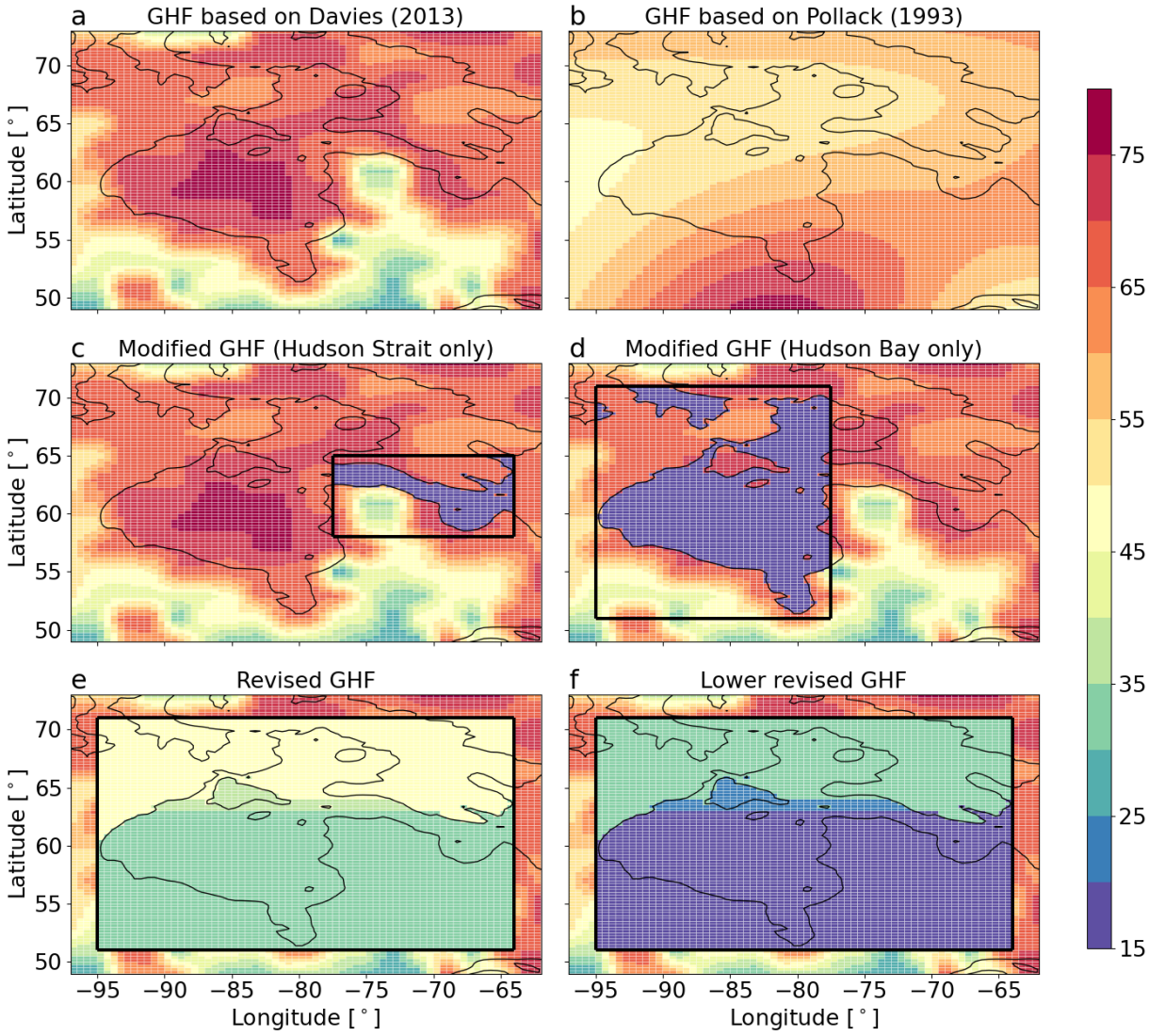

Figure S4. Various GSM input geothermal heat fluxes (GHFs) applied at 4 km depth in mW m^{-2}. The different panels show **a:** default input field (Davies, 2013), **b:** GHF based on Pollack et al. (1993) **c:** same as panel a but with a decreased GHF in Hudson Strait, **d:** same as a but with a decreased GHF in Hudson Bay, **e:** GHF modified based on the GHF map of Blackwell and Richards (2004, $\mathrm{GHF_{ave}} \approx 35\,\mathrm{mW\,m^{-2}}$), **f:** same as panel e but with a 15 mW m^{-2} reduced GHF in the black box ($\mathrm{GHF_{ave}} \approx 20\,\mathrm{mW\,m^{-2}}$). The black contour line shows the present-day sea level used in the GSM.

S4 Additional ocean temperature forcings

S4.1 Ice shelf removal

To calculate the HE shelf forcing, we first define a rectangular function for the i'th HE according to

$$T_{\mathrm{HE,i}} = \begin{cases} T_{\mathrm{max,HE}} & \text{if } \; t_{\mathrm{HE,i,start}} \leq t \leq t_{\mathrm{HE,i,end}} \\ 0 & \text{otherwise,} \end{cases} \tag{S1}$$

where $T_{\mathrm{max,HE}} = [-2, 1, 2, 3]$°C are the maximum ocean temperature anomalies tested (amplitudes based on Gibb et al., 2014). t is the time ranging from 0 to 100 kyr with a 100 yr increment, and $t_{\mathrm{HE,i,start}}$ and $t_{\mathrm{HE,i,end}}$ are the start and end time of the i'th HE. The timing and duration of HEs are based on the average of Table 6.3 in Bradley (2014). For HEs without an estimated duration, we use 1 kyr (centered around the HE time estimate). To get a more gradual ocean temperature increase and decrease, we convolute $T_{\mathrm{HE,i}}$ with a Gaussian function of the form

$$y_{\mathrm{Gauss,i,tmp}} = \exp\left(\frac{-x_{\mathrm{Gauss,i}}^2}{2}\right) \tag{S2a}$$

$$y_{\mathrm{Gauss,i}} = \frac{y_{\mathrm{Gauss,i,tmp}}}{\max\left(y_{\mathrm{Gauss,i,tmp}}\right)} \cdot T_{\mathrm{max,HE}}, \tag{S2b}$$

where $x_{\mathrm{Gauss,i}}$ ranges from -10π to 10π over the duration of the i'th HE and is 0 otherwise. The convoluted time series of the i'th HE is then

$$T_{\mathrm{HE,i,conv}} = \begin{cases} T_{\mathrm{HE,i}} * y_{\mathrm{Gauss,i}} & \text{if } \; t_{\mathrm{HE,i,start}} \leq t \leq t_{\mathrm{HE,i,end}} \\ 0 & \text{otherwise.} \end{cases} \tag{S3}$$

The final HE shelf forcing time series is obtained by adding the contributions of all individual HEs.

$$T_{\mathrm{HE}} = \sum_i T_{\mathrm{HE,i,conv}}. \tag{S4}$$

Since individual HEs do not overlap, the maximum ocean temperature increase does not exceed $T_{\mathrm{max,HE}}$.

S4.2 Sub-surface ocean warming

The ocean temperature anomalies (OTAs) last for a total of $t_{\mathrm{D,tot}} = 2200$ yr, with an $t_{\mathrm{Inc}} = 1600$ yr long temperature increase and $t_{\mathrm{Dec}} = 600$ yr decrease. According to Rasmussen and Thomsen (2004), the rapid DO climate warmings occur when the water column destabilizes and the warm sub-surface water rises to the surface. Since the warm sub-surface water is then mixed with the cold surface water (decreasing the sub-surface temperature), we align the maximum sub-surface temperature increase of the OTAs with the DO event time estimates (Fig. 3). Following the above, the OTA attributed to the i'th DO event is calculated according to

$$T_{\mathrm{DO,i}} = \begin{cases} T_{\mathrm{max,DO}} \cdot \sin\left(\frac{\pi}{2} \frac{t_{\mathrm{Inc}} - (t - t_{\mathrm{DO,i}})}{t_{\mathrm{Inc}}}\right) & \text{if } \; t_{\mathrm{DO,i}} \leq t \leq t_{\mathrm{DO,i}} + t_{\mathrm{Inc}} \\ T_{\mathrm{max,DO}} \cdot \sin\left(\frac{\pi}{2} \frac{t_{\mathrm{Dec}} - (t_{\mathrm{DO,i}} - t)}{t_{\mathrm{Dec}}}\right) & \text{if } \; t_{\mathrm{DO,i}} - t_{\mathrm{Dec}} \leq t < t_{\mathrm{DO,i}} \\ 0 & \text{otherwise,} \end{cases} \tag{S5}$$

where $t_{\mathrm{DO,i}}$ is the time of the i'th DO event. Note that due to the implementation of the OTAs in Eq. S5, the values of $T_{DO,i}$ at $t_{\mathrm{DO,i}} + t_{\mathrm{Inc}}$ and $t_{\mathrm{DO,i}} - t_{\mathrm{Dec}}$ are 0°C. For a time step of 100 yr, the actual duration of increased sub-surface water temperature is, therefore, $t_{\mathrm{D}} = 2000$ yr. Following Bassis et al. (2017), the contributions of overlapping OTAs are added

$$T_{\mathrm{DO}} = \sum_i T_{\mathrm{DO,i}} \tag{S6}$$

Therefore, T_{DO} can exceed $T_{\mathrm{max,DO}}$ (Fig. 3).

S5 Ensemble parameter ranges

	Number - Definition	Parameter	initial range	range of sieved ensemble	scaling and unit
a	01 - Weertman soft-bed sliding coefficient	C_{rmu} (Eq. 3a)	$0.10 \rightarrow 2.00$	$0.25 \rightarrow 1.90$	$R \cdot \frac{3\ \mathrm{m\,yr^{-1}}}{(30\ \mathrm{kPa})^{n_{\mathrm{b,soft}}}}$
	02 - Weertman hard-bed sliding coefficient	C_{slid} (Eq. 3b)	$0.20 \rightarrow 4.99$	$0.24 \rightarrow 4.98$	$R \cdot \frac{3\ \mathrm{m\,yr^{-1}}}{(30\ \mathrm{kPa})^4}$
	34 - exponent for grid cell fractional sediment cover	fbedpow	$0.00 \rightarrow 1.00$	$0.04 \rightarrow 0.88$	$R \cdot 3.8 + 0.2$
	35 - basal drag soft bed subgrid roughness dependency	$F_{\mathrm{sub,till}}$ (Eq. 3a)	$0.00 \rightarrow 1.00$	$0.01 \rightarrow 0.87$	
	36 - basal drag hard bed subgrid roughness dependency	$F_{\mathrm{sub,slid}}$ (Eq. 3b)	$0.00 \rightarrow 1.00$	$0.03 \rightarrow 0.91$	
	37 - soft bed Weertman sliding exponent	$n_{\mathrm{b,soft}}$ (Eq. 1)	$1 \rightarrow 7$	$1 \rightarrow 7$	integer values only
	38 - Glen flow law enhancement	fnflow	$2.50 \rightarrow 4.00$	$2.55 \rightarrow 3.69$	
	42 - Coulomb-plastic friction coefficient	C_{c} (Eq. 6)	$1.00 \rightarrow 4.60$	$3.12 \rightarrow 4.59$	if $R < 3.1 \rightarrow 0$, else $\rightarrow R - 3$
b	03 - calving coefficent	fcalvin	$0.10 \rightarrow 0.70$	$0.39 \rightarrow 0.65$	$R \cdot 10\ \mathrm{km\,yr^{-1}}$
	04 - hydrofracturing coefficient	pfactdwCrack	$0.51 \rightarrow 4.00$	$0.67 \rightarrow 3.96$	$R \cdot 100$
	05 - face melt coefficient	C_{face} (Eq. 10)	$0.50 \rightarrow 4.00$	$0.54 \rightarrow 2.88$	$R \cdot 10\ \mathrm{m\,yr^{-1}}$
	06 - sub-shelf melt coefficient	C_{SSM} (Eq. 9)	$0.00 \rightarrow 0.80$	$0.00 \rightarrow 0.71$	$R \cdot 16 + 2$
	07 - marine freezing point (effective bias adjustment)	TssmCut	$0.00 \rightarrow 1.00$	$0.12 \rightarrow 0.98$	$-R \cdot 4^{\circ}\mathrm{C}$
	41 - ocean temperature glacial index phase factor	rToceanPhase	$0.50 \rightarrow 2.00$	$0.50 \rightarrow 1.97$	
c	08 - global precipitation scale factor for PMIP component	fnpre	$0.80 \rightarrow 1.80$	$0.88 \rightarrow 1.73$	
	09 - precipitation orographic forcing regularization	pREG	$0.00 \rightarrow 1.00$	$0.06 \rightarrow 0.99$	$1 \cdot 10^{-3} \cdot 40^{R}$
	11 - precipitation glacial index phase factor	fnPdexp	$0.51 \rightarrow 1.94$	$0.80 \rightarrow 1.48$	
	23 - south-central precipitation enhancement factor	fmpreSM	$0.00 \rightarrow 1.00$	$0.25 \rightarrow 0.94$	
	24 - orographic control parameter	rtdes	$0.00 \rightarrow 1.00$	$0.08 \rightarrow 0.93$	
	26 - weight of glacially-indexed input GCM precipitation field	fPREweightPMIP	$0.00 \rightarrow 1.00$	$0.02 \rightarrow 0.93$	
d	10 - coefficient for exponential surface temperature dependence of non-PMIP precipitation	fhPRE	$0.03 \rightarrow 0.97$	$0.05 \rightarrow 0.66$	$R \cdot 0.1$
	12 - global LGM temperature scale factor	fnTdfscale	$0.75 \rightarrow 1.25$	$1.03 \rightarrow 1.23$	
	13 - temperature glacial index phase factor	fnTdexp	$0.75 \rightarrow 1.25$	$0.75 \rightarrow 1.05$	
	25 - LGM environmental lapse rate	rlapseIgm	$0.00 \rightarrow 1.00$	$0.02 \rightarrow 0.50$	$R \cdot 4^{\circ}\mathrm{C\,km^{-1}} + 4^{\circ}\mathrm{C\,km^{-1}}$
e	14 - desert-elevation exponent	desFac	$0.50 \rightarrow 2.00$	$0.51 \rightarrow 1.91$	
	15 - default desert-elevation cutoff	des2	$0.50 \rightarrow 3.00$	$0.52 \rightarrow 2.89$	km
	16 - western desert-elevation cutoff	desSW	$0.51 \rightarrow 3.00$	$0.89 \rightarrow 2.80$	km
	17 - northwestern desert-elevation cutoff	desNNW	$0.50 \rightarrow 3.00$	$0.84 \rightarrow 2.90$	km
	18 - north-central desert-elevation cutoff	desNC	$0.00 \rightarrow 2.50$	$0.01 \rightarrow 2.45$	km
	19 - central desert-elevation cutoff	desC	$0.00 \rightarrow 2.50$	$0.08 \rightarrow 2.26$	km
	20 - Foxe Basin/Baffin desert-elevation cutoff	desF	$0.00 \rightarrow 2.50$	$0.63 \rightarrow 2.32$	km
	21 - Quebec/Labrador desert-elevation cutoff	desQ	$0.50 \rightarrow 3.63$	$0.64 \rightarrow 2.65$	km
	22 - south-central desert-elevation cutoff	desSC	$0.00 \rightarrow 2.49$	$0.00 \rightarrow 1.98$	km
f	27 - principal Empirical Orthogonal Function (pEOF) weight 1	w_{pEOF1}	$0.00 \rightarrow 1.00$	$0.12 \rightarrow 0.98$	$R - 0.5$
	28 - pEOF weight 2	w_{pEOF2}	$0.00 \rightarrow 1.00$	$0.16 \rightarrow 0.97$	$R - 0.5$
	29 - temporal Empirical Orthogonal Function (tEOF) weight 1	w_{tEOF1}	$0.00 \rightarrow 1.00$	$0.02 \rightarrow 0.57$	$R - 0.5$
	30 - tEOF weight 2	w_{tEOF2}	$0.00 \rightarrow 1.00$	$0.35 \rightarrow 0.90$	$R - 0.5$
g	31 - scaling of EBM temperature field glacial anomaly	fnTEBMscale	$0.90 \rightarrow 1.50$	$0.92 \rightarrow 1.48$	
	32 - weight of EBM temperature field	fTweightEBM	$0.00 \rightarrow 1.00$	$0.01 \rightarrow 0.43$	
	33 - SW surface melt coefficient	fRadSMB	$0.20 \rightarrow 0.50$	$0.20 \rightarrow 0.48$	$R \cdot 2$
	39 - weight of EBM for glacial index setting	rWtEBMindx	$0.00 \rightarrow 1.00$	$0.01 \rightarrow 0.41$	
	40 - weight of annual glacial index from ice core records	wtIndxYr	$0.00 \rightarrow 1.00$	$0.06 \rightarrow 0.98$	
h	43 - effective bed roughness scale	$h_{\mathrm{wb,Crit}}$ (Eq. 5)	$0.00 \rightarrow 1.00$	$0.11 \rightarrow 0.98$	$0.01 \cdot 10^{(2R)}\ \mathrm{m}$
	44 - constant bed drainage rate	$R_{\mathrm{b,drain}}$	$0.00 \rightarrow 1.00$	$0.01 \rightarrow 0.92$	$10^{R} \cdot 10^{-3}\ \mathrm{m\,yr^{-1}}$
	45 - effective-pressure factor	$N_{\mathrm{eff,Fact}}$ (Eq. 4)	$0.00 \rightarrow 1.00$	$0.24 \rightarrow 0.97$	$10^{R} \cdot 2 \cdot 10^{4}\ \mathrm{Pa}$
i	46 - margin forcing ablation threshold	margbab	$0.00 \rightarrow 0.90$	$0.00 \rightarrow 0.90$	
	47 - margin forcing accumulation threshold	margbac	$0.00 \rightarrow 1.00$	$0.00 \rightarrow 0.90$	
	48 - margin forcing calving reduction factor	margcalv	$0.02 \rightarrow 1.00$	$0.02 \rightarrow 1.00$	
	49 - margin forcing initiation time	fmgpin	$0.90 \rightarrow 0.90$	$0.90 \rightarrow 0.90$	$25\ \mathrm{kyr\ BP} + R \cdot 100\ \mathrm{kyr\ BP}$
j	50 - thickness of the Lithosphere	d_{L}	$46.0 \rightarrow 146.$	$46.0 \rightarrow 146.$	km
	51 - viscosity of the upper mantle	η_{um}	$0.20 \rightarrow 2.00$	$0.20 \rightarrow 2.00$	$10^{21}\ \mathrm{Pa\,s}$
	52 - viscosity of the lower mantle	η_{lm}	$1.00 \rightarrow 50.0$	$2.00 \rightarrow 50.0$	$10^{21}\ \mathrm{Pa\,s}$

Table S1. GSM parameter ranges of the initial North American history-matching ensemble (Tarasov et al., 2024; Tarasov and Goldstein, 2021) and the final sieved ensemble used within this study (20 parameter vectors). The individual parameters are grouped into the following themes (from top to bottom): **a** ice dynamics, **b** ice-ocean interactions, **c** precipitation, **d** temperature, **e** desert elevation control, **f** empirical orthogonal functions, **g** energy balance model, **h** basal hydrology model, **i** margin nudging, and **j** glacial isostatic adjustment. The numbers indicate the read-in order of the GSM (matching the input parameter file). R in the last column represents any value within the corresponding parameter range.

S6 Reference ensemble

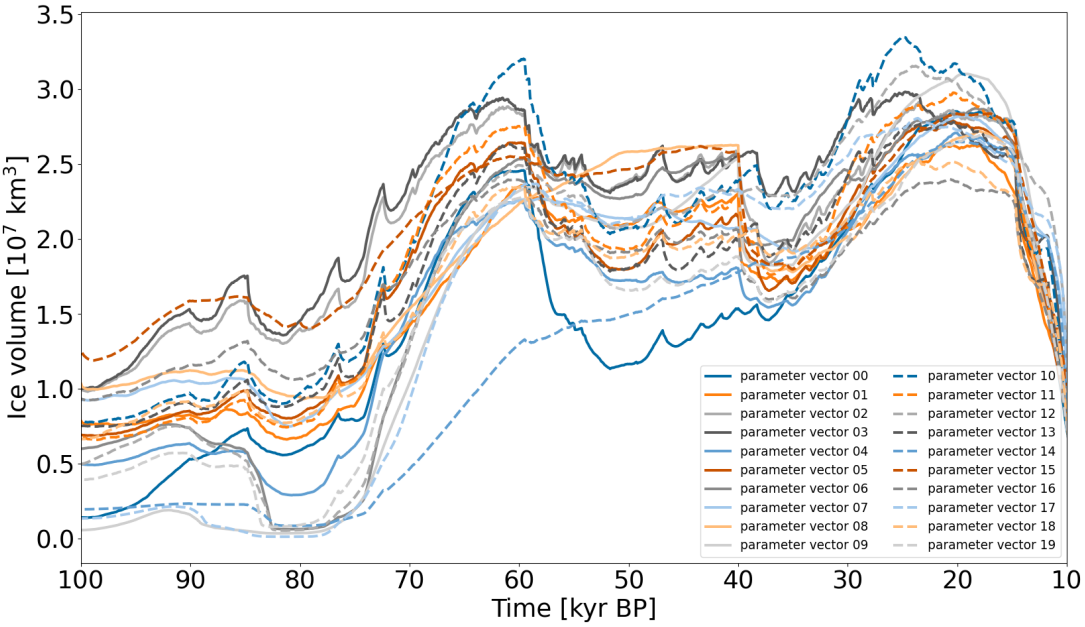

Figure S5. Total North American ice volume for all 20 parameter vectors of the reference ensemble.

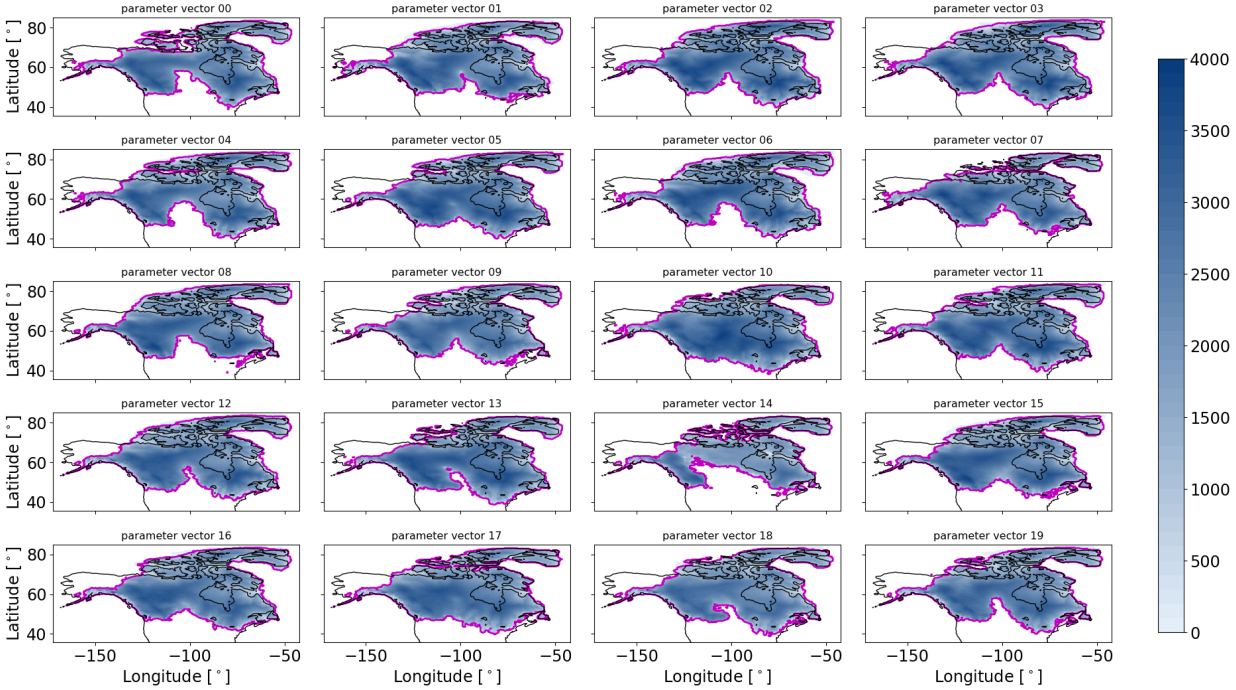

Figure S6. North American ice sheet surface elevation in meters at 60 kyr BP for all 20 parameter vectors of the reference ensemble. The magenta and black contour lines mark the ice sheet extent and the present-day sea level (coastline) used in the GSM, respectively.

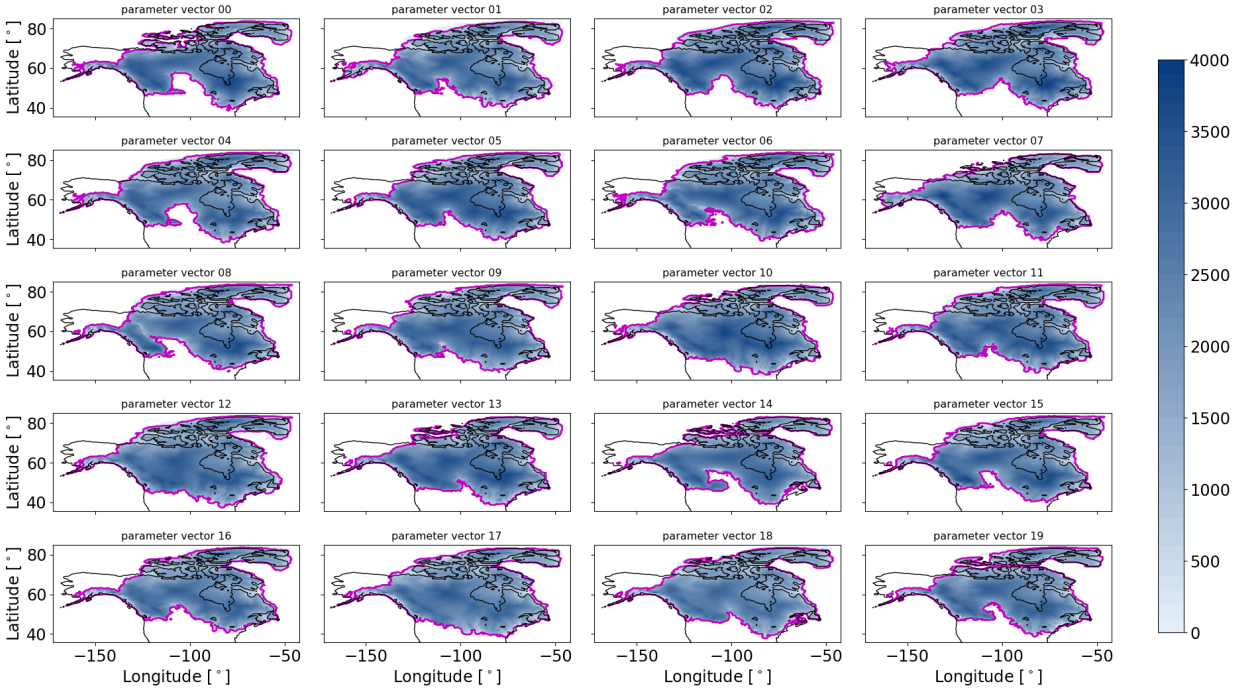

Figure S7. North American ice sheet surface elevation in meters at 24 kyr BP. Otherwise as Fig. S6.

S7 Hudson Strait ice stream surges

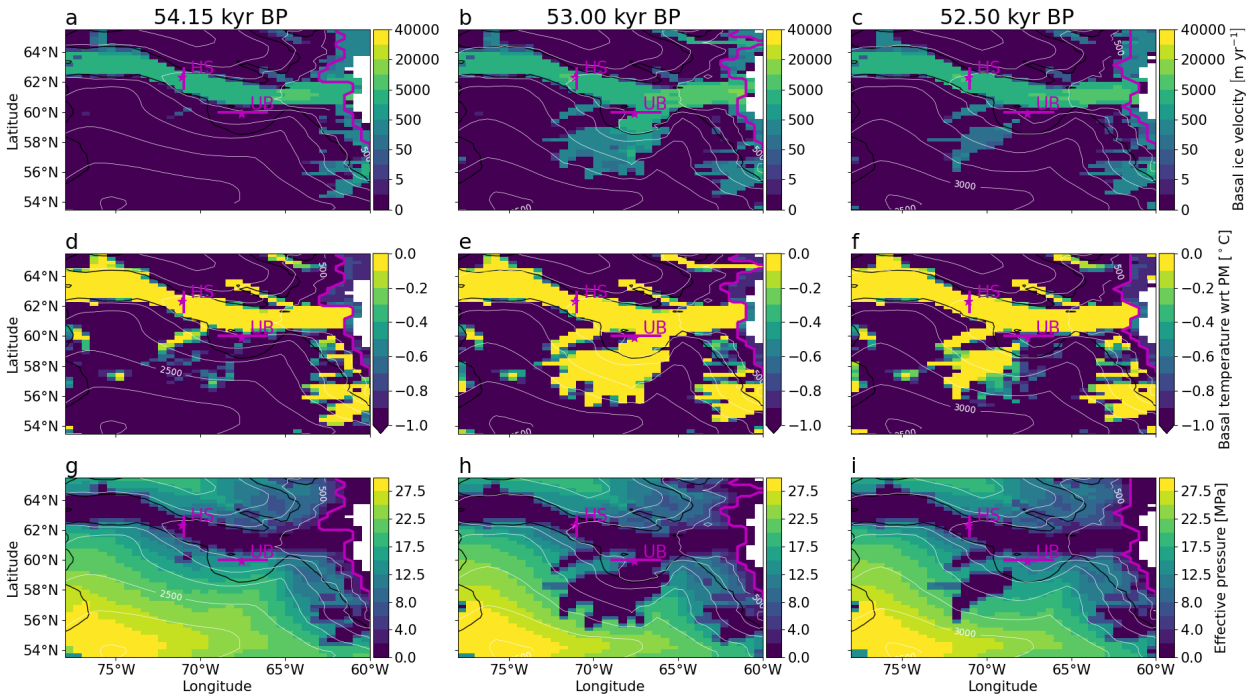

Figure S8. Basal ice velocity (first row), basal temperature with respect to the pressure melting point (second row), and effective pressure (third row) for a surge in Ungava Bay. The 3 time slices (columns) show the active Hudson Strait ice stream before the Ungava Bay surge (54.15 kyr BP), the Ungava Bay surge (53.00 kyr BP), and the active Hudson Strait ice stream after the Ungava Bay surge (52.50 kyr BP). The magenta asterisks and lines indicate the location of Hudson Strait (*HS*) and Ungava Bay (*UB*) ice thickness calculation and flux gate, respectively. The magenta and white contour lines represent the grounding line and ice sheet surface elevation in meters, respectively. The black contour is the present-day sea level (coastline) used in the GSM.

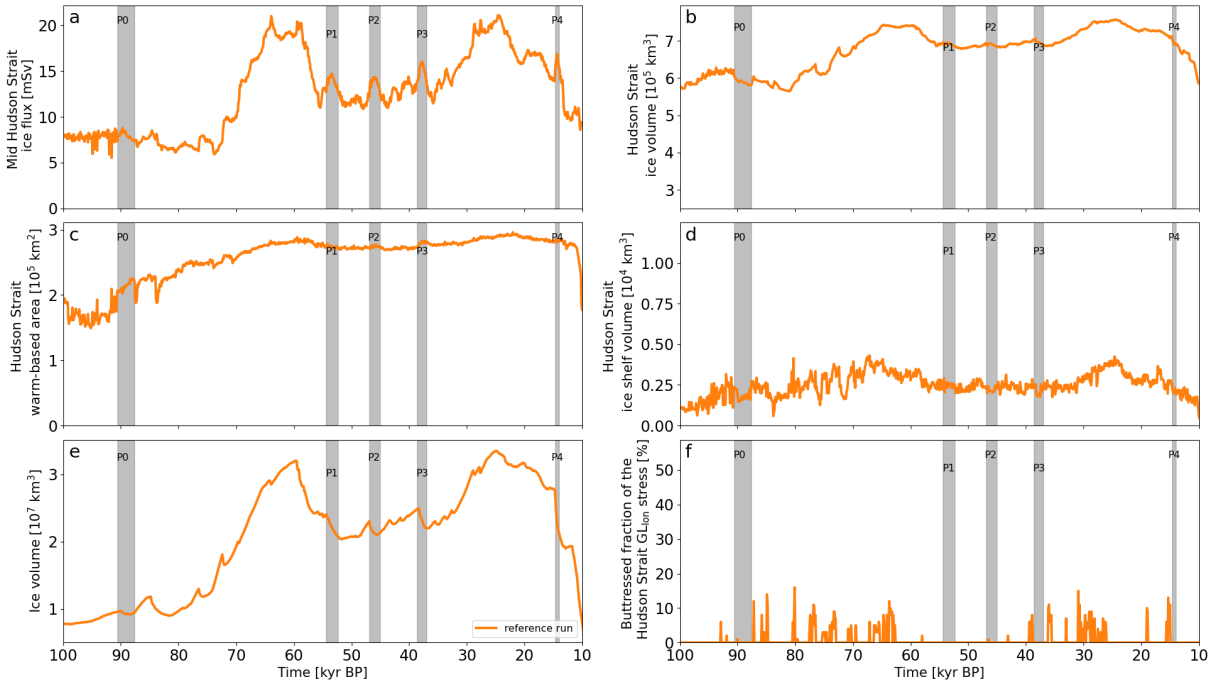

Figure S9. Time series of parameter vector 10. Panel e shows the overall North American ice volume. Otherwise as Fig. 4.

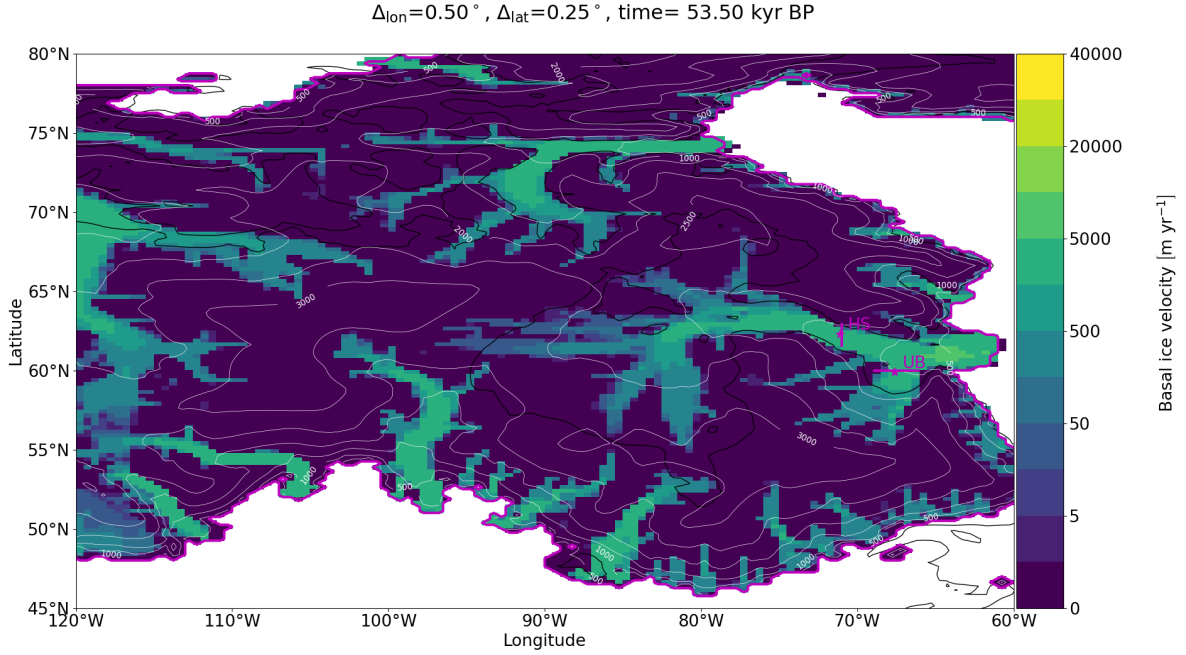

Figure S10. Basal ice velocity during surge P1 for parameter vector 10 in Fig. S9. The magenta contour line represents the grounding line. The black contour is the present-day sea level (coastline) used in the GSM.

S7.1 Timing of Hudson Strait surges

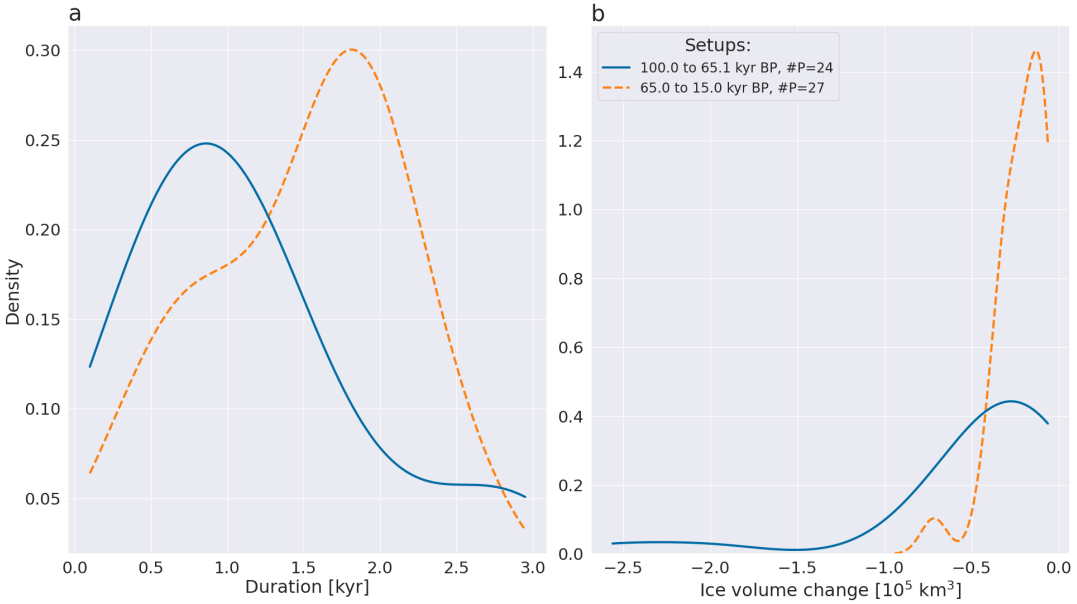

Figure S11. Kernel density plot for the whole ensemble (reference setup) and 2 different periods. #P indicates the total number of surges across all runs of the ensemble.

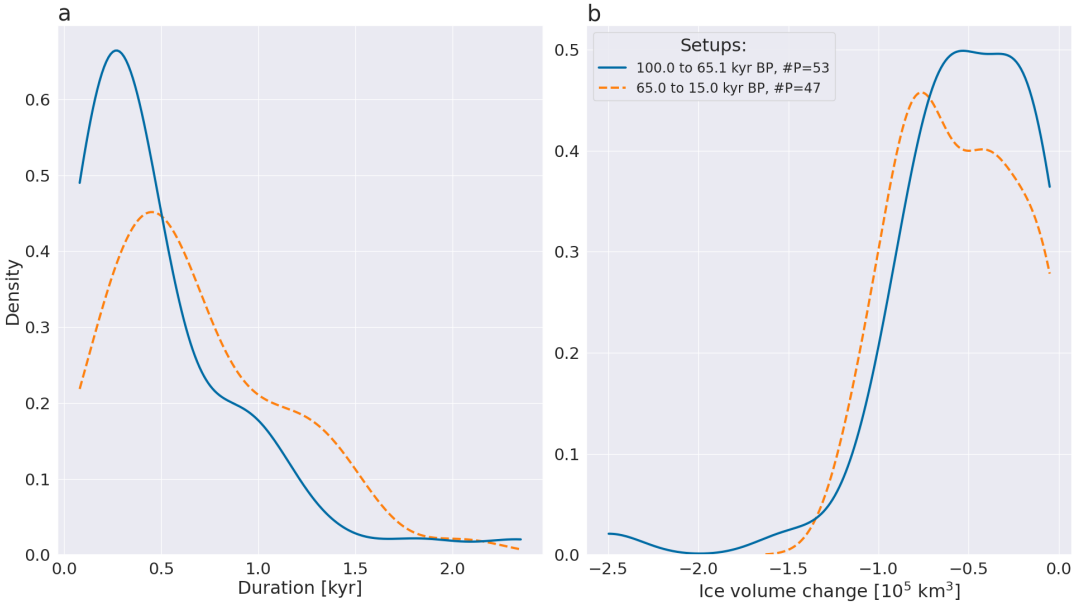

Figure S12. Kernel density plot for the whole ensemble of the $\mathrm{GHF}_{\mathrm{ave}} = 25\,\mathrm{mW\,m^{-2}}$ experiments and 2 different periods. #P indicates the total number of surges across all runs of the ensemble.

S7.2 Effects of a lower geothermal heat flux

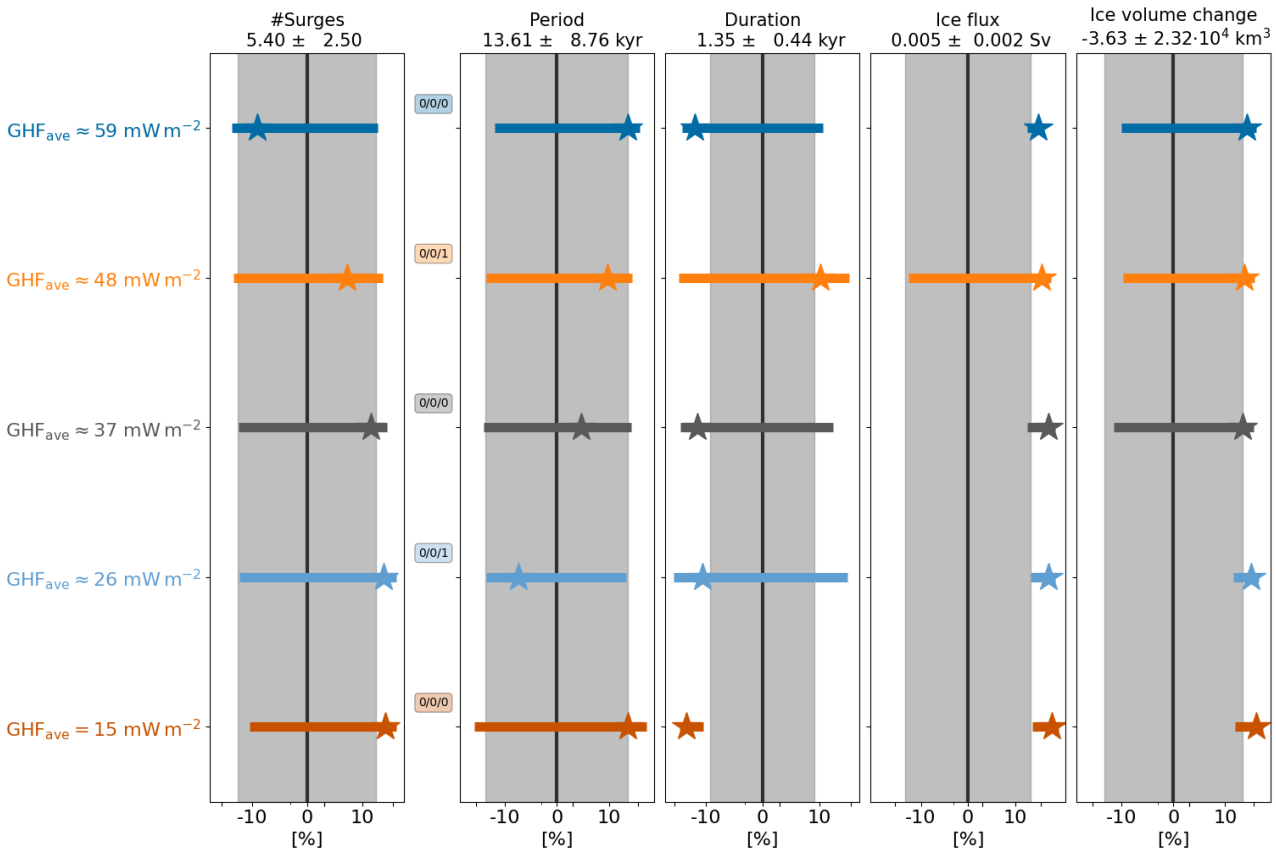

Figure S13. Percentage differences in surge characteristics compared to the reference setup. Only parameter vectors within the #surges > 2 sub-ensemble are considered. The model setups, from top to bottom, are $\mathrm{GHF}_{\mathrm{ave}} \approx [15, 26, 37, 48, 59]\,\mathrm{mW\,m^{-2}}$ (Sec. 2.2). Otherwise as Fig. 6

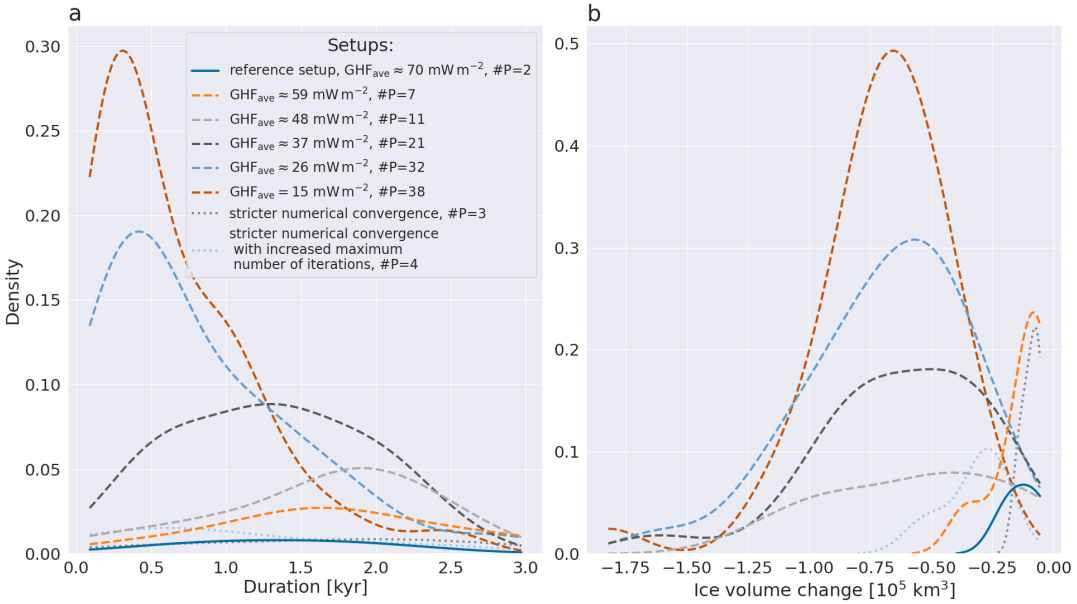

Figure S14. Kernel density plot for different $\mathrm{GHF_{ave}}$ for the #surges ≤ 2 sub-ensemble. The reference and MNEEs setups use $\mathrm{GHF_{ave}} \approx 70\,\mathrm{mW\,m^{-2}}$. #P indicates the total number of surges across all runs of the sub-ensemble.

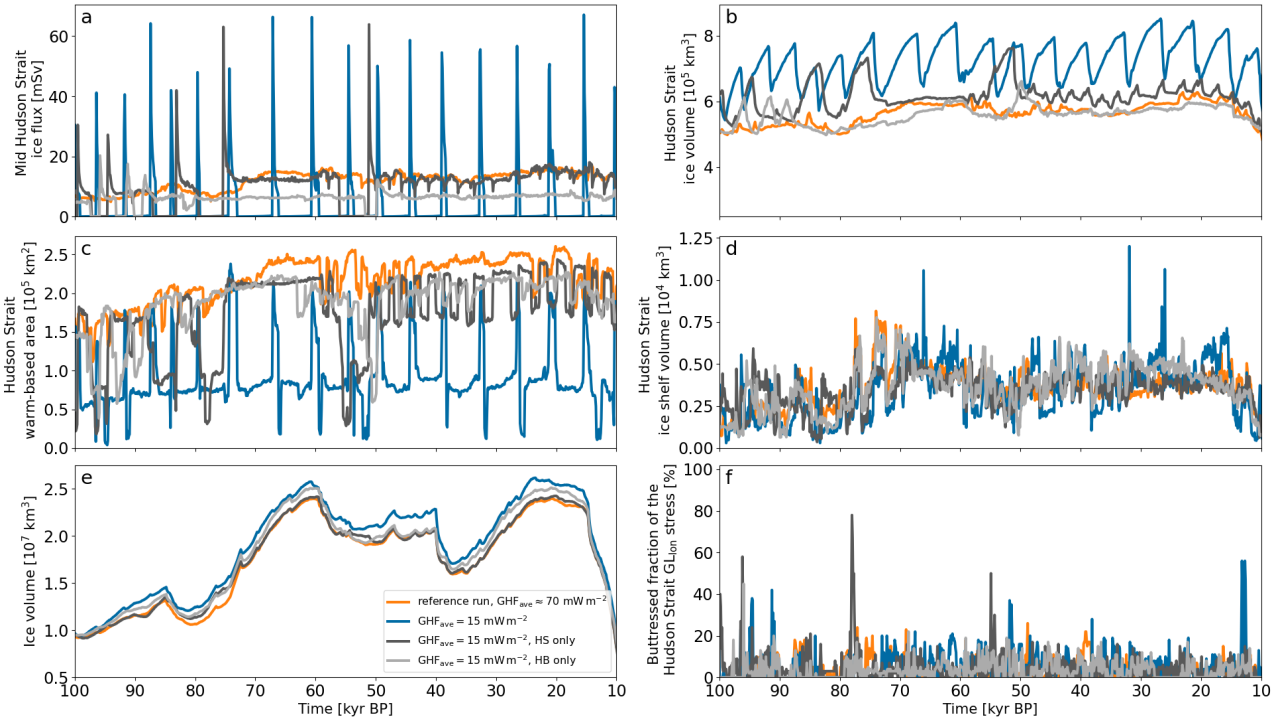

Figure S15. Time series of parameter vector 16 for different GHF modification regions (Sec. 2.2, Fig. 1 and S4c,d). The Hudson Strait ice stream surges are not highlighted for clarity. Panel e shows the overall North American ice volume. Otherwise as Fig. 4.

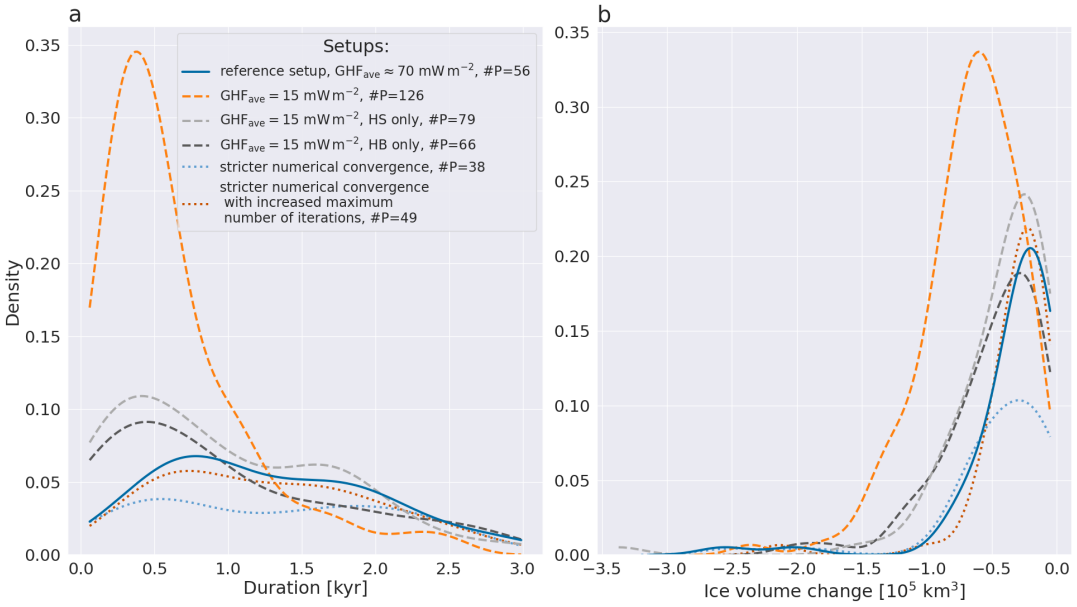

Figure S16. Kernel density plot for the whole ensemble. The reference and MNEEs setups use $\mathrm{GHF_{ave}} \approx 70\,\mathrm{mW\,m^{-2}}$. The GHF modification is applied separately to the Hudson Strait (Fig. S4c) and Hudson Bay (Fig. S4d) for the *HS only* and *HB only* setup, respectively. #P indicates the total number of surges across all runs of the ensemble.

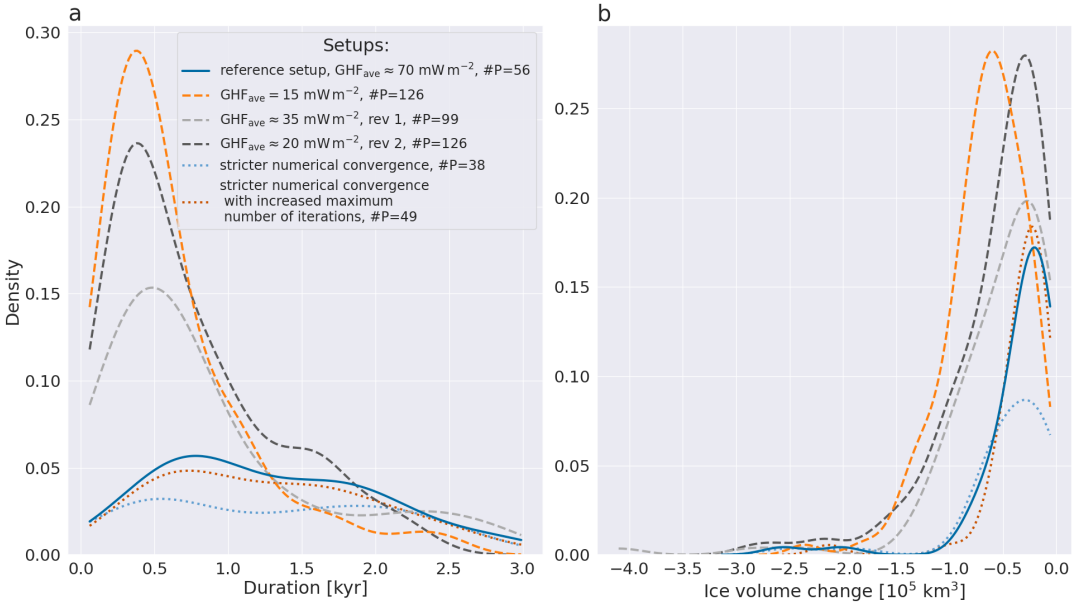

Figure S17. Kernel density plot for the whole ensemble. The reference and MNEEs setups use $\mathrm{GHF_{ave}} \approx 70\,\mathrm{mW\,m^{-2}}$. The GHF modification for $\mathrm{GHF_{ave}} = 15\,\mathrm{mW\,m^{-2}}$ is applied to the Hudson Strait and Hudson Bay (Fig. 1b). $\mathrm{GHF_{ave}} \approx 35\,\mathrm{mW\,m^{-2}}$, rev 1 and $\mathrm{GHF_{ave}} \approx 20\,\mathrm{mW\,m^{-2}}$, rev 2 use the GHF maps shown in panels e and f of Fig. S4, respectively. #P indicates the total number of surges across all runs of the ensemble.

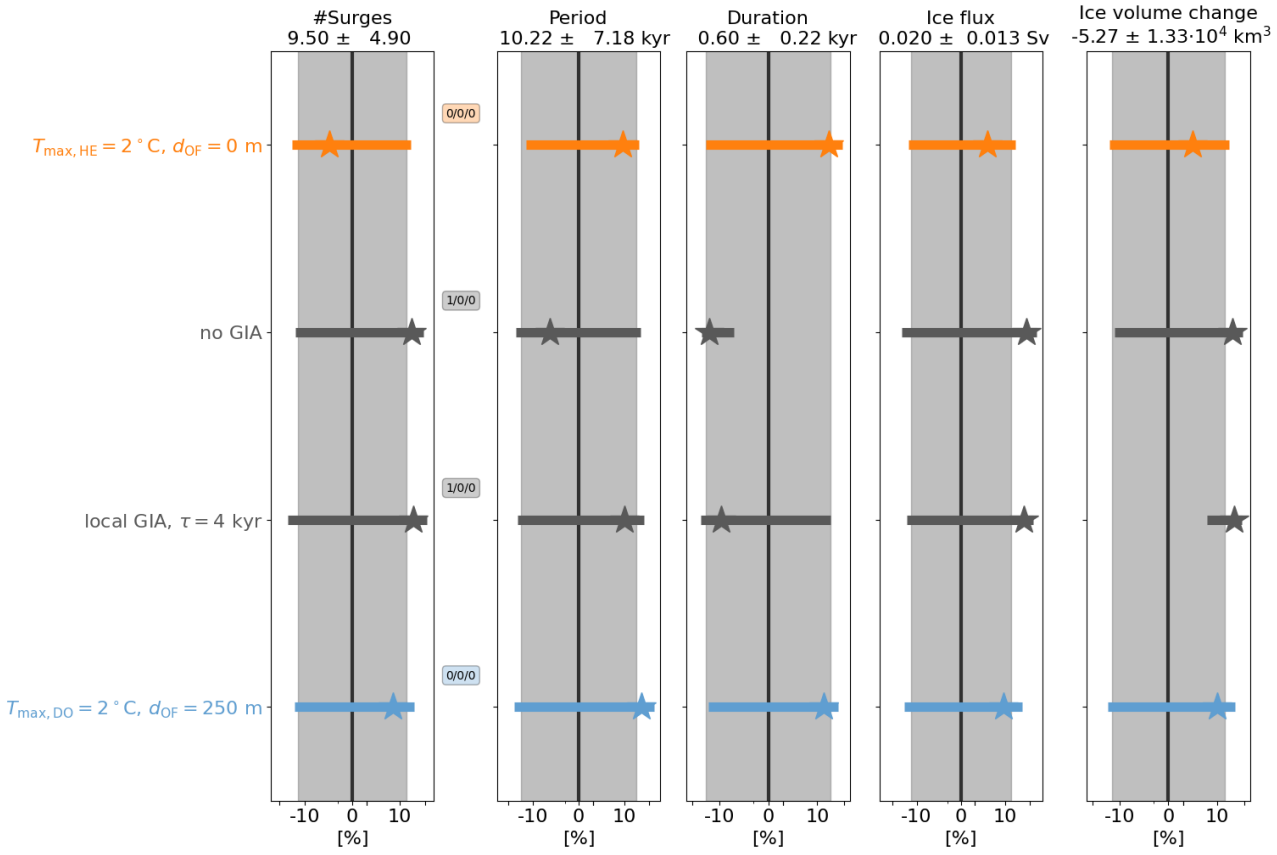

Figure S18. Percentage differences in surge characteristics compared to the $\mathrm{GHF}_{\mathrm{ave}} = 25\,\mathrm{mW\,m^{-2}}$ setup for the #surges > 2 sub-ensemble (11 parameter vectors). All comparison setups also use $\mathrm{GHF}_{\mathrm{ave}} = 25\,\mathrm{mW\,m^{-2}}$. The model setups, from top to bottom, are: Heinrich Event ocean forcing ($T_{\mathrm{max,HE}} = 2°\mathrm{C}$, $d_{\mathrm{OF}} = 0\,\mathrm{m}$), no GIA model, local GIA model with relaxation time constant $\tau = 4\,\mathrm{kyr}$, DO event sub-surface ocean forcing with $T_{\mathrm{max,DO}} = 2°\mathrm{C}$. Otherwise as Fig. 6.

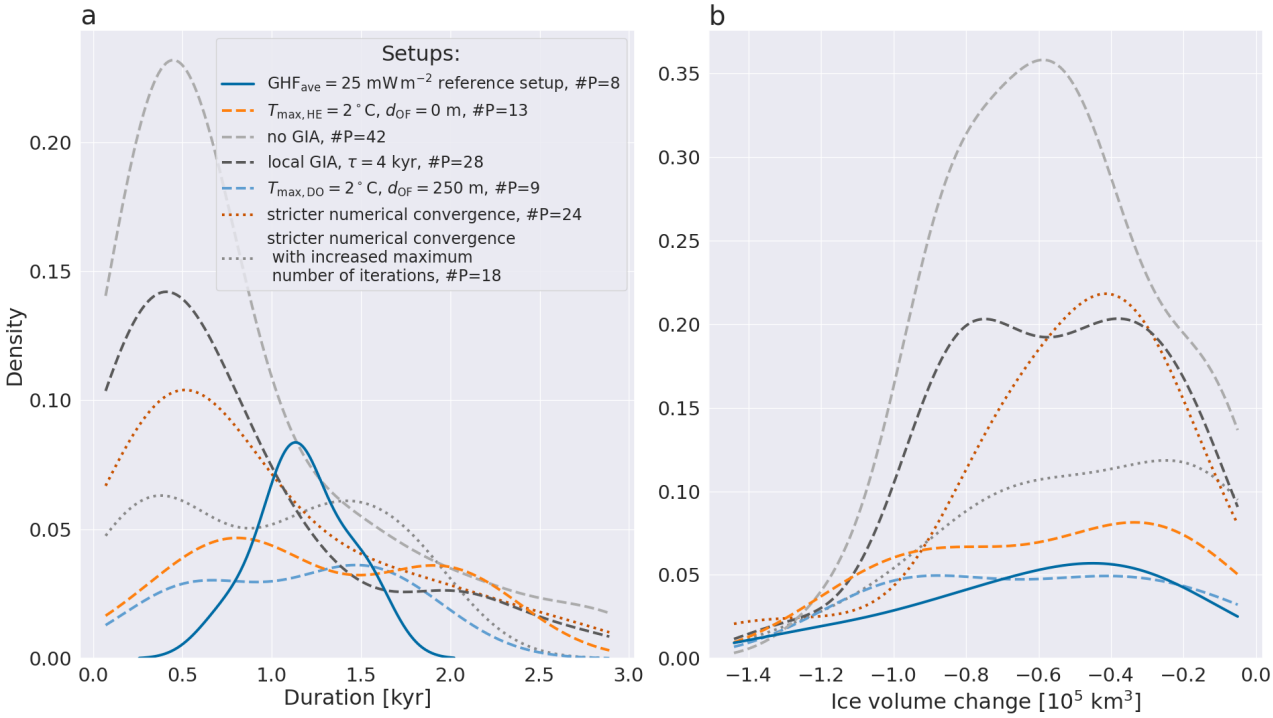

Figure S19. Kernel density plot for the #surges ≤ 2 sub-ensemble (9 parameter vectors) of the $\mathrm{GHF_{ave}} = 25\,\mathrm{mW\,m^{-2}}$ experiments (used in all setups shown). #P indicates the total number of surges across all runs of the sub-ensemble.

S7.3 Effects of a different sliding law

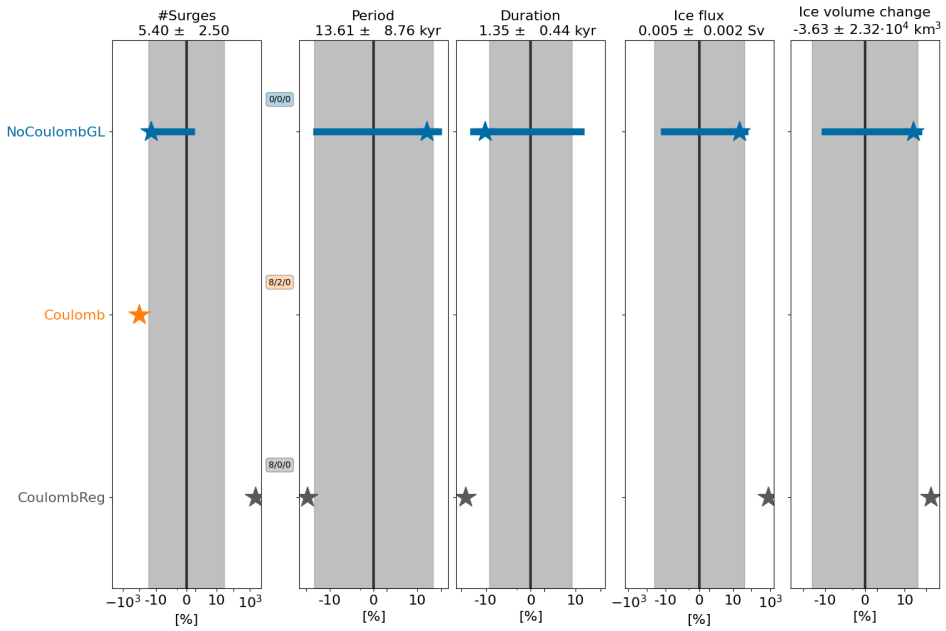

Figure S20. Percentage differences in surge characteristics compared to the reference setup for the #surges > 2 sub-ensemble. The model setups, from top to bottom, are: pure Weertman-type grounding line parameterization ($\tau_{b,GL} = \tau_{b,W}$ instead of Eq. 7), Coulomb friction law (Eq. 6a), and regularized Coulomb friction law (Eq. 6b). Otherwise as Fig. 6.

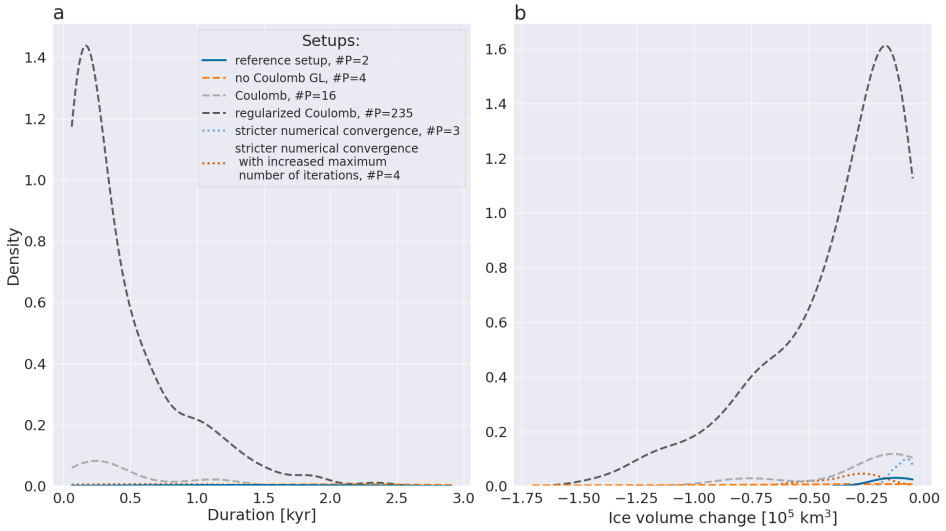

Figure S21. Kernel density plot for the #surges ≤ 2 sub-ensemble. #P indicates the total number of surges across all runs of the sub-ensemble. The model setups, from top to bottom, are: reference setup, pure Weertman-type grounding line parameterization ($\tau_{b,GL} = \tau_{b,W}$ instead of Eq. 7), Coulomb friction law (Eq. 6a), regularized Coulomb friction law (Eq. 6b), and the 2 MNEE experiments.

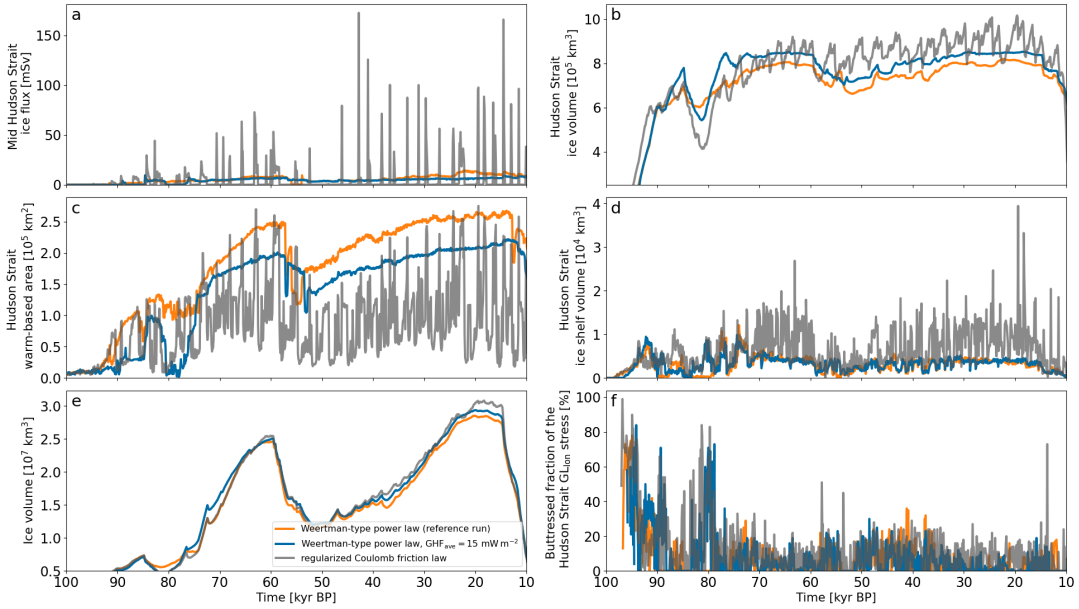

Figure S22. Time series of parameter vector 0 for different sliding laws (Weertman-type power law exponent is 4) and geothermal heat fluxes. The Hudson Strait ice stream surges are not highlighted for clarity. Panel e shows the overall North American ice volume. Otherwise as Fig. 4.

S8 Ocean temperature forcing experiments

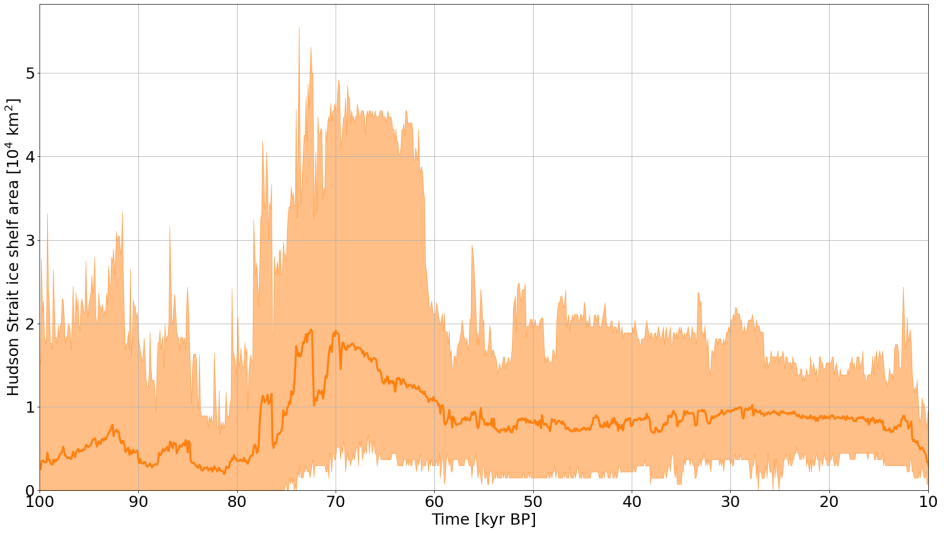

Figure S23. Hudson Strait ice shelf cover in the *ice shelf area* outlined in Fig. 2 (total area of $\sim 2.6 \cdot 10^5$ km^2). The thick line represents the mean of the 20 run ensemble. The shaded area marks the minimum and maximum of the ensemble.

S8.1 Ice shelf removal

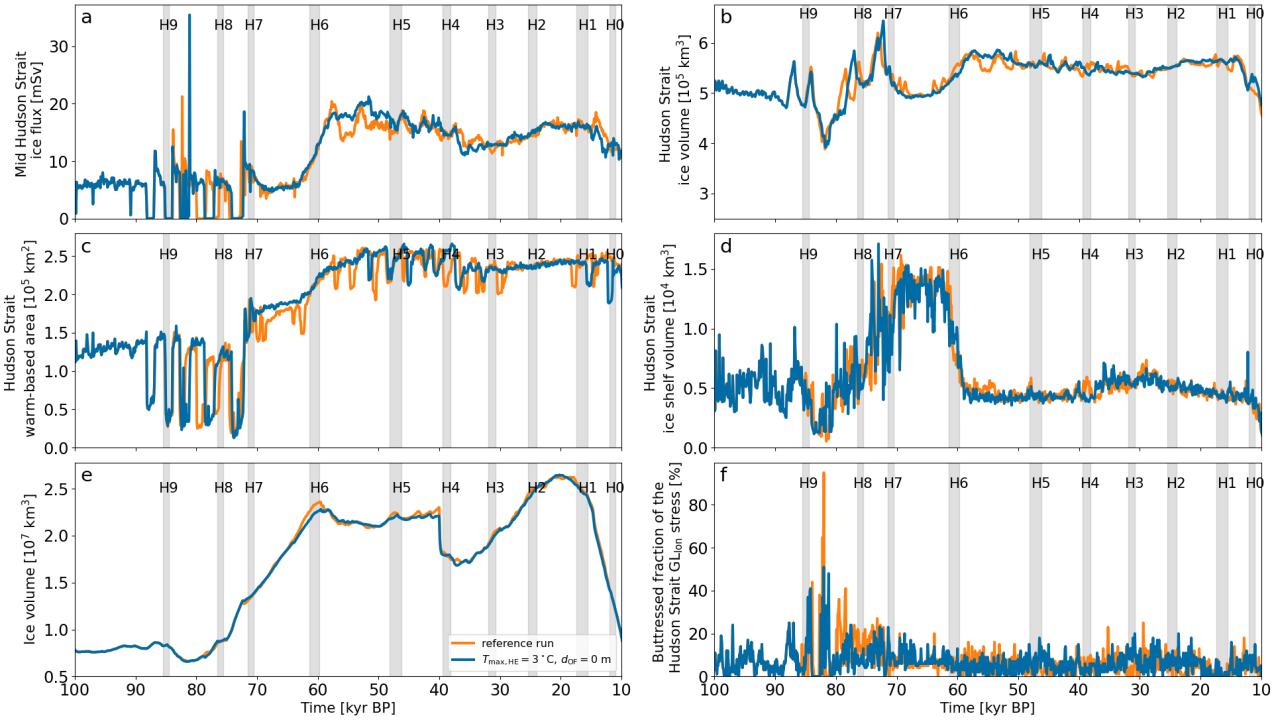

Figure S24. Time series of parameter vector 1 for the reference setup and the ice shelf removal ocean forcing (Sec. 2.3.1). The shaded gray areas mark the HE time estimates based on the average of Table 6.3 in Bradley (2014). The ocean forcing was applied to the whole water column ($d_{\mathrm{OF}} = 0$ m) and with a maximum temperature increase of $T_{\mathrm{max,HE}} = 3°\mathrm{C}$. Panel e shows the overall North American ice volume. Otherwise as Fig. 4.

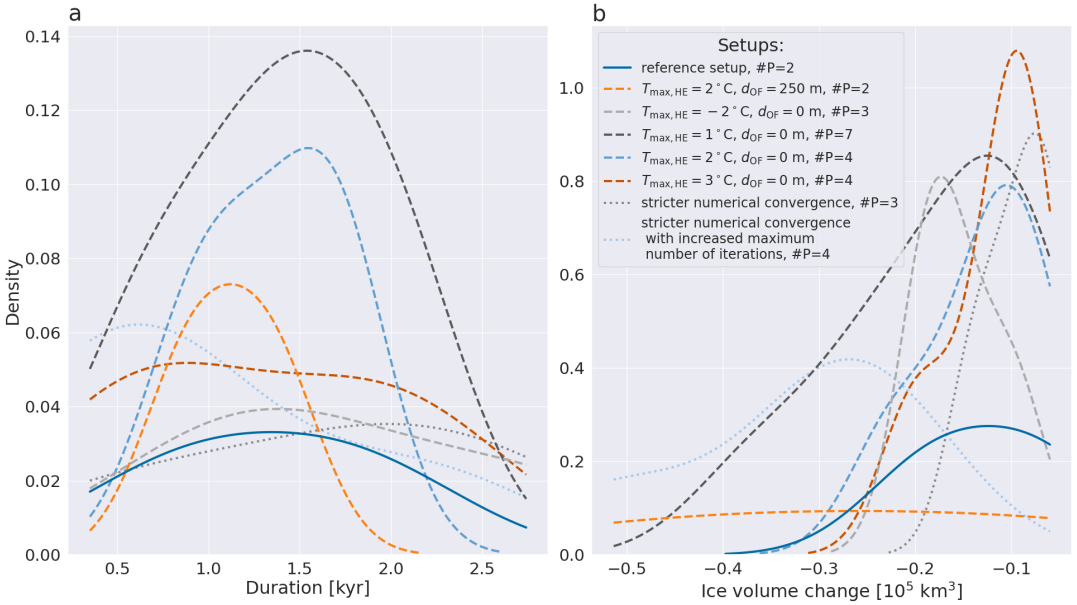

Figure S25. Kernel density plot for the #surges ≤ 2 sub-ensemble. The model setups, from top to bottom, are the reference setup, Heinrich Event ocean forcings (maximum temperature increase $T_{\mathrm{max,HE}} = 2°\mathrm{C}$, $d_{\mathrm{OF}} = 250$ m), whole water column Heirich Event ocean forcing with $T_{\mathrm{max,HE}} = [-2, 1, 2, 3]°\mathrm{C}$ (Sec. 2.3.1) and the 2 MNEE experiments. #P indicates the total number of surges across all runs of the sub-ensemble.

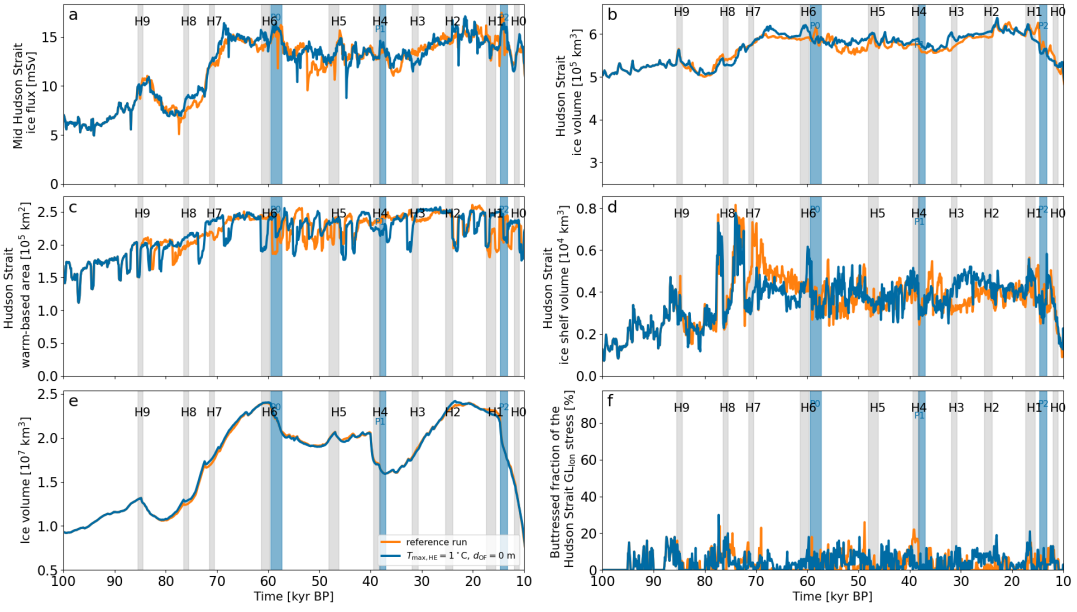

Figure S26. Time series of parameter vector 16 for the reference setup and the ice shelf removal ocean forcing (Sec. 2.3.1). The shaded gray areas mark the HE time estimates based on the average of Table 6.3 in Bradley (2014). The ocean forcing was applied to the whole water column ($d_{\mathrm{OF}} = 0$ m) and with a maximum temperature increase of $T_{\mathrm{max,HE}} = 1°\mathrm{C}$. Panel e shows the overall North American ice volume. Otherwise as Fig. 4.

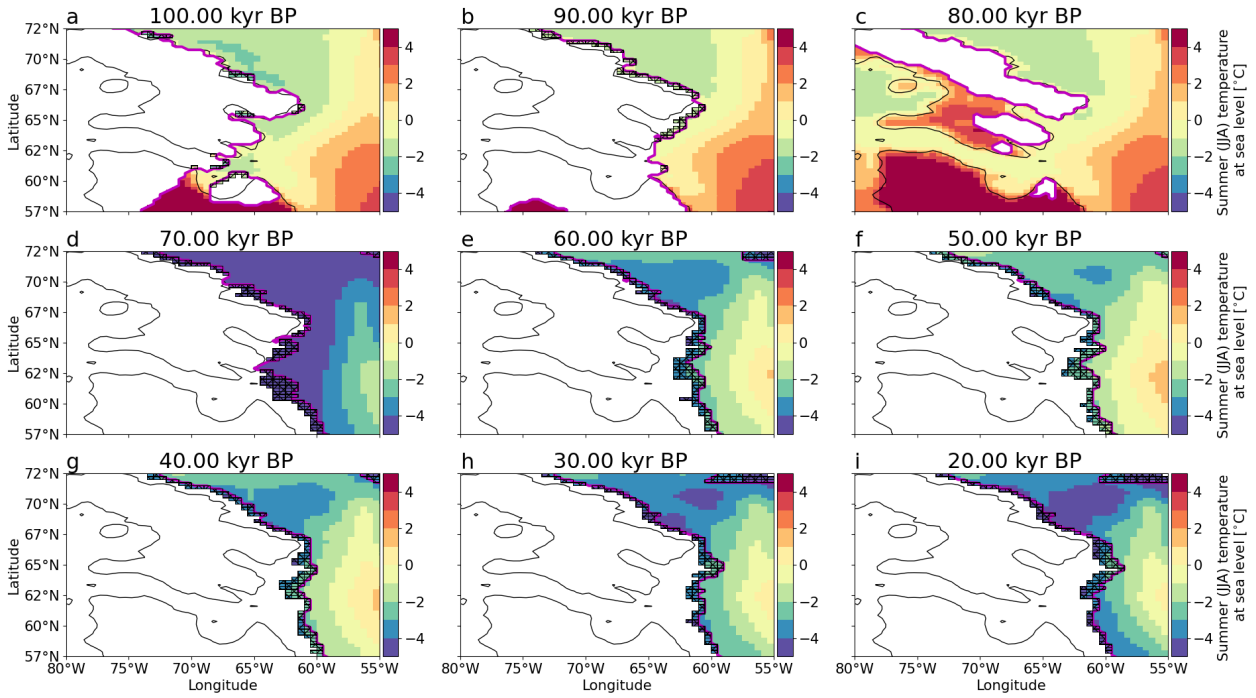

Figure S27. 2 m summer surface temperature for parameter vector 2 (not shown for grid cells with grounded ice). The magenta contour line and black hatches represent the ice margin and floating ice shelves, respectively. The black contour is the present-day sea level (coastline) used in the GSM.

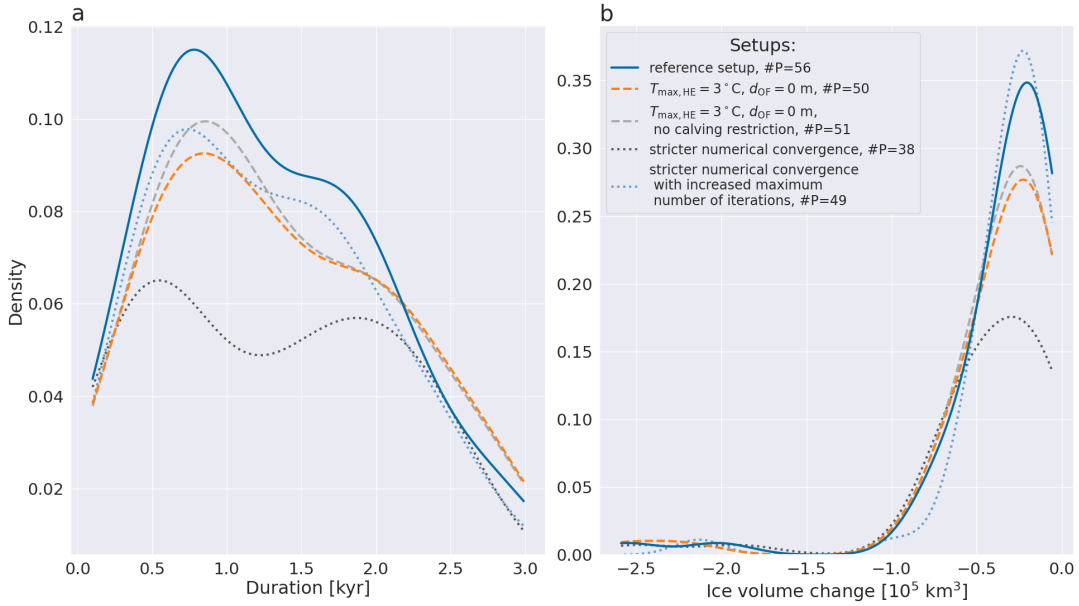

Figure S28. Kernel density plot for the whole ensemble. The $T_{\max,\mathrm{HE}} = 3°\mathrm{C}$, $d_{\mathrm{OF}} = 0$ m setup inhibits calving when the 2 m summer surface temperature is below $-2.0°\mathrm{C}$ (see Sec. 2.3 for details). #P indicates the total number of surges across all runs of the ensemble.

S8.2 Adding underwater warming pulses

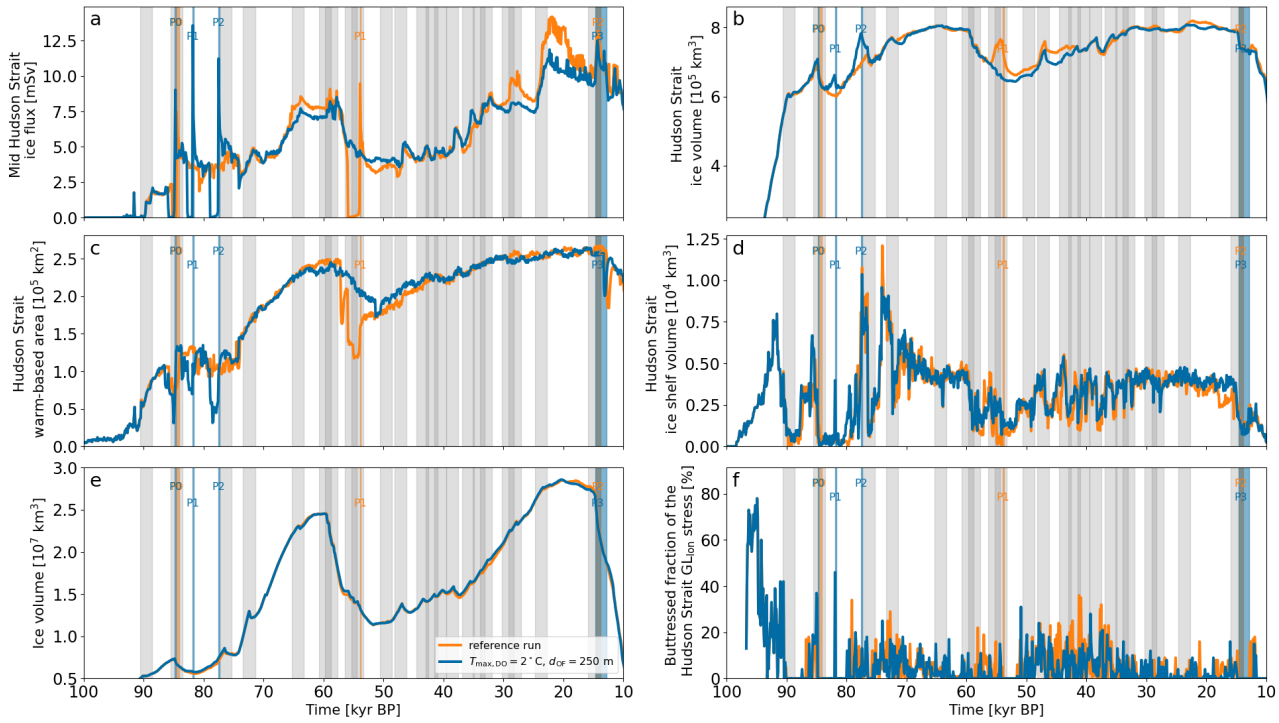

Figure S29. Time series of parameter vector 0 for the reference setup and the sub-surface ocean forcing (Sec. 2.3.2). The shaded gray areas mark the DO event time estimates based on peaks in the NGRIP δ^{18}O time series (Bazin et al., 2013; Veres et al., 2013) with a total duration of $t_{\mathrm{D,tot}} = 2200$ yr (Sec. S4.2). The darker gray areas indicate an overlap of sub-surface ocean warmings. The ocean forcing was applied below a water depth of $d_{\mathrm{OF}} = 250$ m and with a maximum temperature increase of $T_{\mathrm{max,DO}} = 2^{\circ}$C. Panel e shows the overall North American ice volume. Otherwise as Fig. 4.

S8.3 End-member scenarios

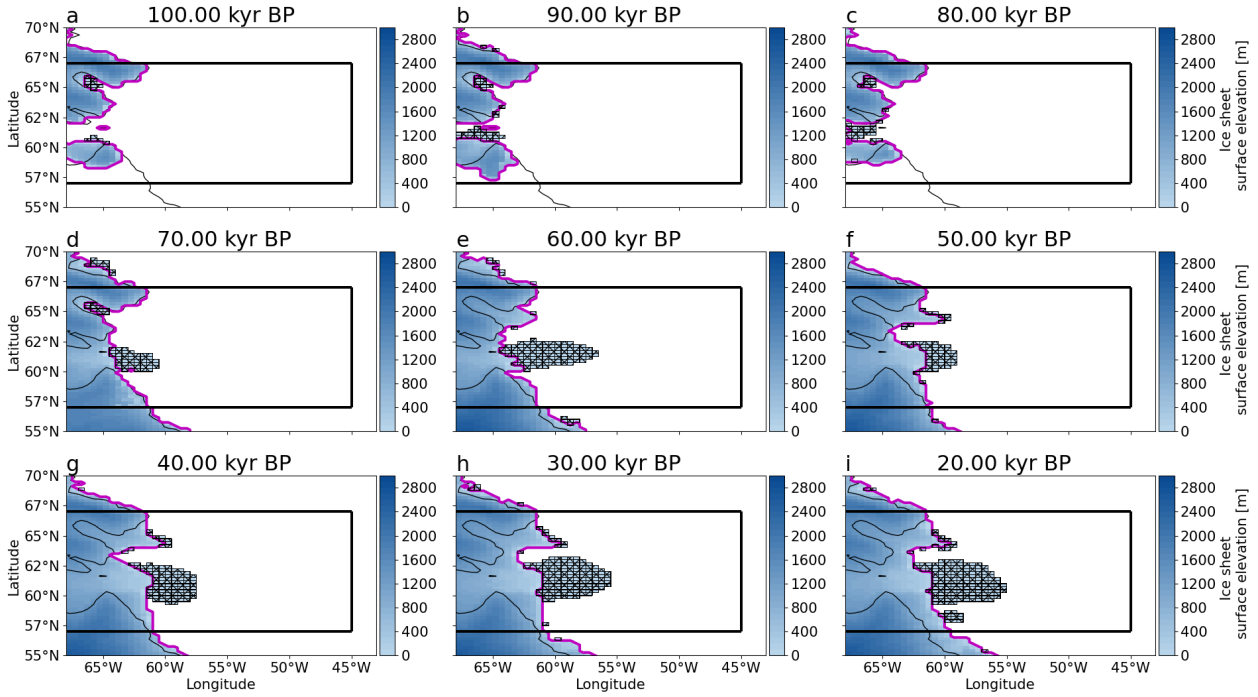

Figure S30. Ice surface elevation in meters for parameter vector 14 and no calving in the *ocean forcing area* (black box, see also Fig. 2). The magenta contour line and black hatches represent the grounding line and floating ice shelves, respectively. The black contour is the present-day sea level (coastline) used in the GSM.

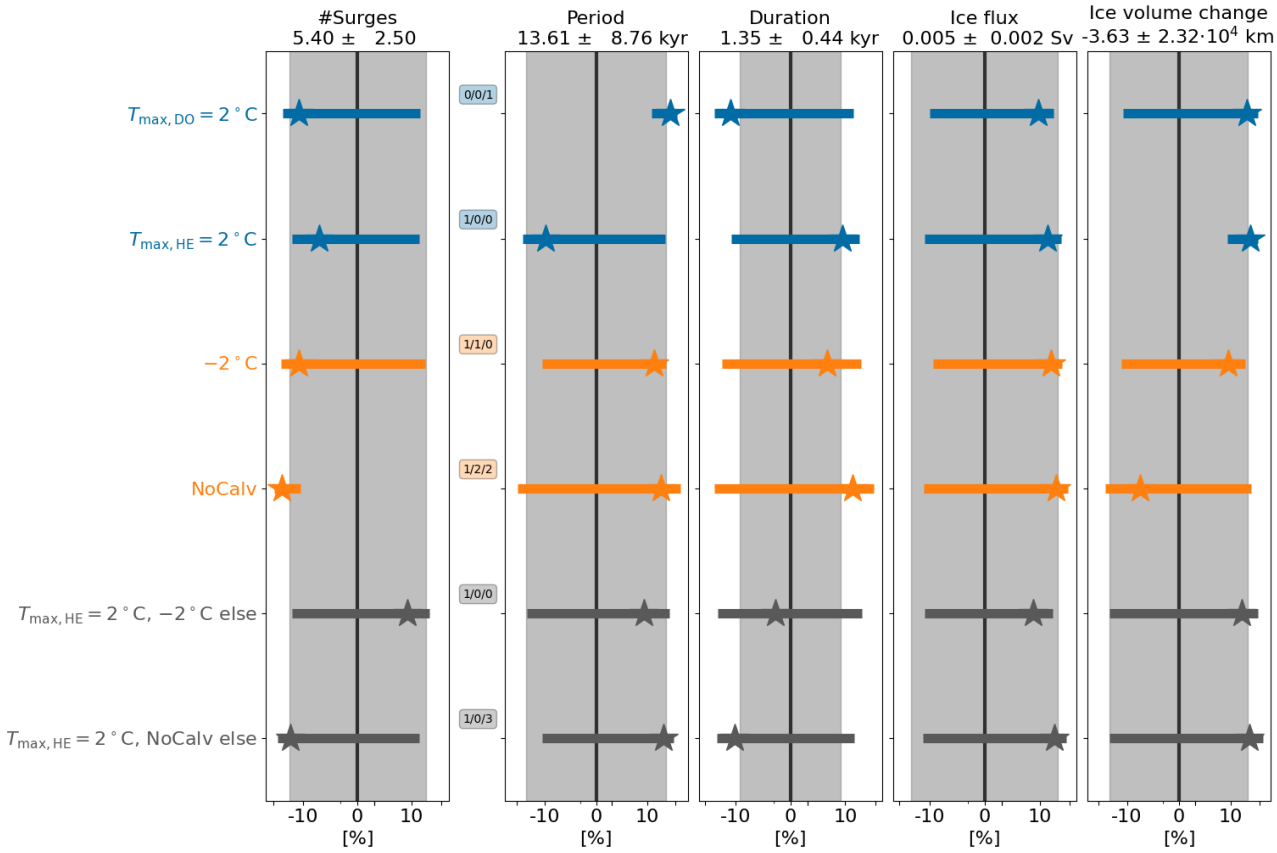

Figure S31. Percentage differences in surge characteristics compared to the reference setup. Only parameter vectors within the #surges > 2 sub-ensemble are considered. The model setups, from top to bottom, are the end-member scenario experiments (Sec. 2.3.3): DO event ocean forcing with maximum temperature increase $T_{\mathrm{max,DO}} = 2°\mathrm{C}$ (EMS_1), HE ocean forcing with maximum temperature increase $T_{\mathrm{max,HE}} = 2°\mathrm{C}$ (EMS_2), $-2°\mathrm{C}$ ocean temperature decrease applied after 100 kyr BP (EMS_3), no calving after 100 kyr BP (EMS_4), HE ocean forcing ($T_{\mathrm{max,HE}} = 2°\mathrm{C}$) with $-2°\mathrm{C}$ ocean forcing applied outside of HEs and after 100 kyr BP (EMS_5), and HE ocean forcing ($T_{\mathrm{max,HE}} = 2°\mathrm{C}$) with no calving outside of HEs and after 100 kyr BP (EMS_6). The ocean forcings are applied for the entire water column ($d_{\mathrm{OF}} = 0$ m) and all grid cells within the *ocean forcing area* (not only the ones containing floating ice, Sec. 2.3.3). Otherwise as Fig. 6.

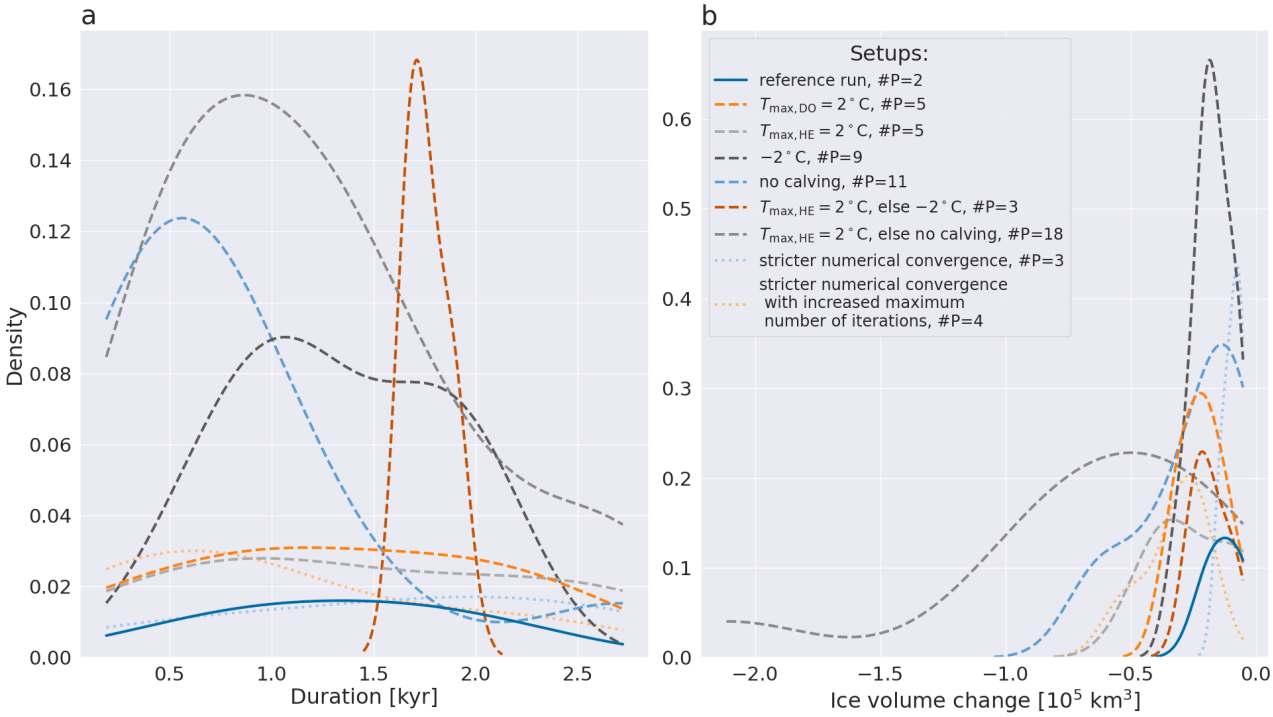

Figure S32. Kernel density plot for the #surges ≤ 2 sub-ensemble. The model setups, from top to bottom, are the reference setup, DO event ocean forcing with maximum temperature increase $T_{\mathrm{max,DO}} = 2°\mathrm{C}$ (EMS_1), HE ocean forcing with maximum temperature increase $T_{\mathrm{max,HE}} = 2°\mathrm{C}$ (EMS_2), $-2°\mathrm{C}$ ocean temperature decrease applied after 100 kyr BP (EMS_3), no calving after 100 kyr BP (EMS_4), HE ocean forcing ($T_{\mathrm{max,HE}} = 2°\mathrm{C}$) with $-2°\mathrm{C}$ ocean forcing applied outside of HEs and after 100 kyr BP (EMS_5), HE ocean forcing ($T_{\mathrm{max,HE}} = 2°\mathrm{C}$) with no calving outside of HEs and after 100 kyr BP (EMS_6), and the 2 MNEE experiments. The ocean forcings are applied for the entire water column ($d_{\mathrm{OF}} = 0$ m) and all grid cells within the *ocean forcing area* (not only the ones containing floating ice, Sec. 2.3.3). #P indicates the total number of surges across all runs of the sub-ensemble.

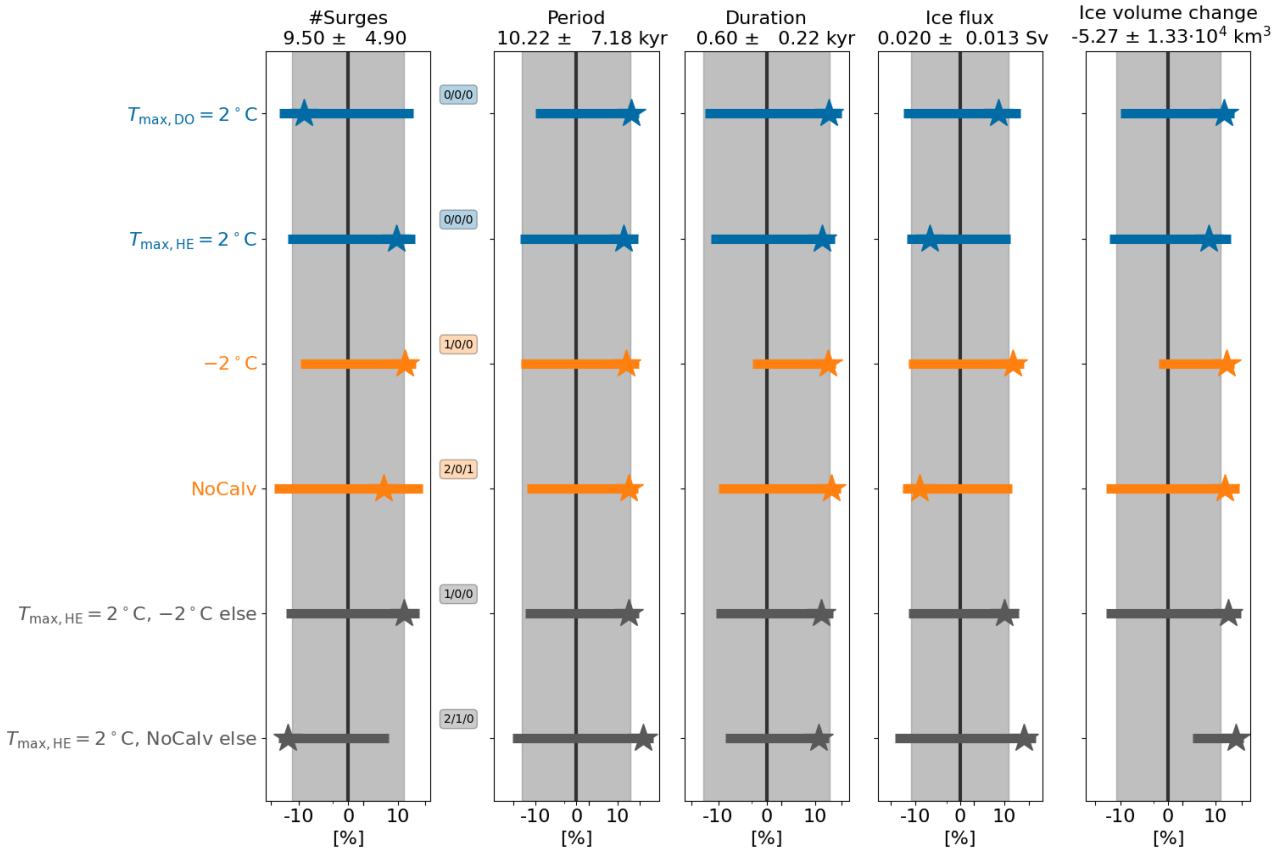

Figure S33. Percentage differences in surge characteristics compared to the $\mathrm{GHF_{ave}} = 25\,\mathrm{mW\,m^{-2}}$ reference setup for the #surges > 2 sub-ensemble (11 parameter vectors). All comparison setups also use $\mathrm{GHF_{ave}} = 25\,\mathrm{mW\,m^{-2}}$. The model setups, from top to bottom, are the end-member scenario experiments (Sec. 2.3.3): DO event ocean forcing with maximum temperature increase $T_{\mathrm{max,DO}} = 2^{\circ}\mathrm{C}$ ($\mathrm{EMS_1}$), HE ocean forcing with maximum temperature increase $T_{\mathrm{max,HE}} = 2^{\circ}\mathrm{C}$ ($\mathrm{EMS_2}$), $-2^{\circ}\mathrm{C}$ ocean temperature decrease applied after 100 kyr BP ($\mathrm{EMS_3}$), no calving after 100 kyr BP ($\mathrm{EMS_4}$), HE ocean forcing ($T_{\mathrm{max,HE}} = 2^{\circ}\mathrm{C}$) with $-2^{\circ}\mathrm{C}$ ocean forcing applied outside of HEs and after 100 kyr BP ($\mathrm{EMS_5}$), and HE ocean forcing ($T_{\mathrm{max,HE}} = 2^{\circ}\mathrm{C}$) with no calving outside of HEs and after 100 kyr BP ($\mathrm{EMS_6}$). The ocean forcings are applied for the entire water column ($d_{\mathrm{OF}} = 0$ m) and all grid cells within the *ocean forcing area* (not only the ones containing floating ice, Sec. 2.3.3). Otherwise as Fig. 6.

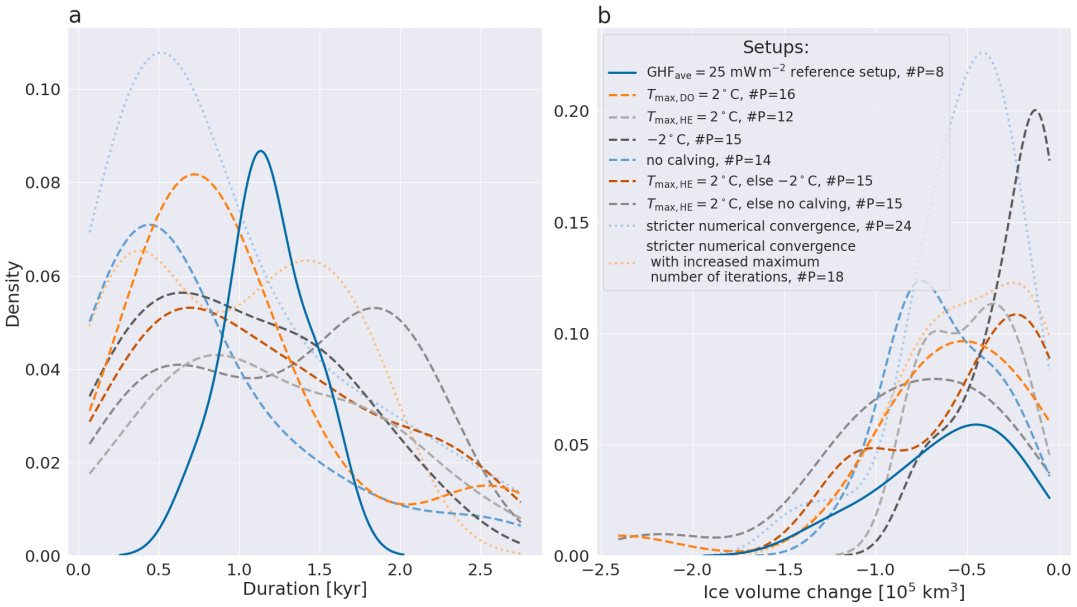

Figure S34. Kernel density plot for the #surges ≤ 2 sub-ensemble with $\mathrm{GHF_{ave}} = 25\,\mathrm{mW\,m^{-2}}$ (9 parameter vectors). The model setups, from top to bottom, are the $\mathrm{GHF_{ave}} = 25\,\mathrm{mW\,m^{-2}}$ reference setup, DO event ocean forcing with maximum temperature increase $T_{\mathrm{max,DO}} = 2°\mathrm{C}$ ($\mathrm{EMS_1}$), HE ocean forcing with maximum temperature increase $T_{\mathrm{max,HE}} = 2°\mathrm{C}$ ($\mathrm{EMS_2}$), $-2°\mathrm{C}$ ocean temperature decrease applied after 100 kyr BP ($\mathrm{EMS_3}$), no calving after 100 kyr BP ($\mathrm{EMS_4}$), HE ocean forcing ($T_{\mathrm{max,HE}} = 2°\mathrm{C}$) with $-2°\mathrm{C}$ ocean forcing applied outside of HEs and after 100 kyr BP ($\mathrm{EMS_5}$), HE ocean forcing ($T_{\mathrm{max,HE}} = 2°\mathrm{C}$) with no calving outside of HEs and after 100 kyr BP ($\mathrm{EMS_6}$), and the 2 MNEE experiments. All setups use $\mathrm{GHF_{ave}} = 25\,\mathrm{mW\,m^{-2}}$. The ocean forcings are applied for the entire water column ($d_{\mathrm{OF}} = 0$ m) and all grid cells within the *ocean forcing area* (not only the ones containing floating ice, Sec. 2.3.3). #P indicates the total number of surges across all runs of the sub-ensemble.

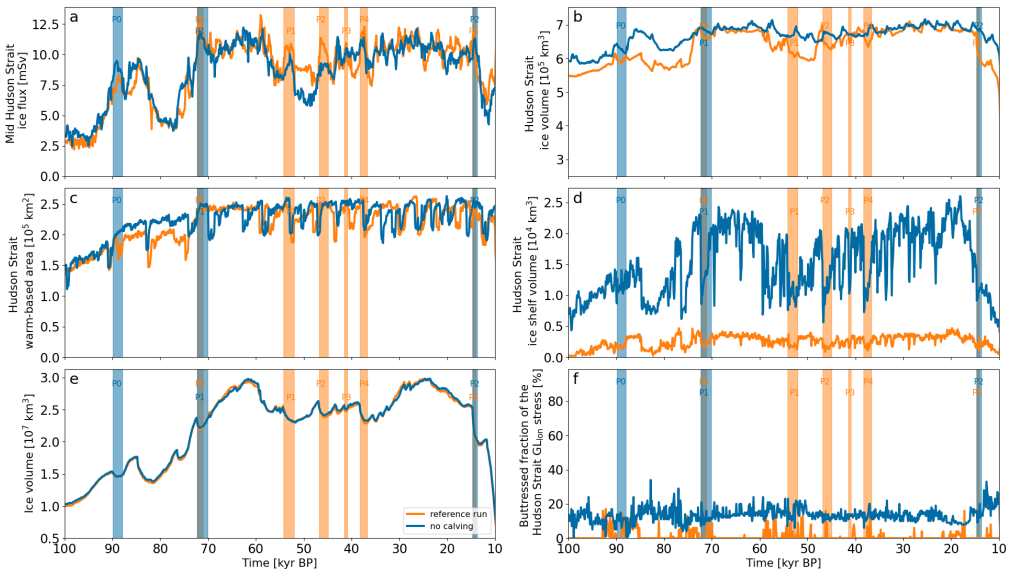

Figure S35. Time series of parameter vector 3 for the reference setup and a run without calving in the *ocean forcing area* after 100 kyr BP ($\mathrm{EMS_4}$ in Sec. 2.3.3). Panel e shows the overall North American ice volume. Otherwise as Fig. 4.

S9 Glacial isostatic adjustment

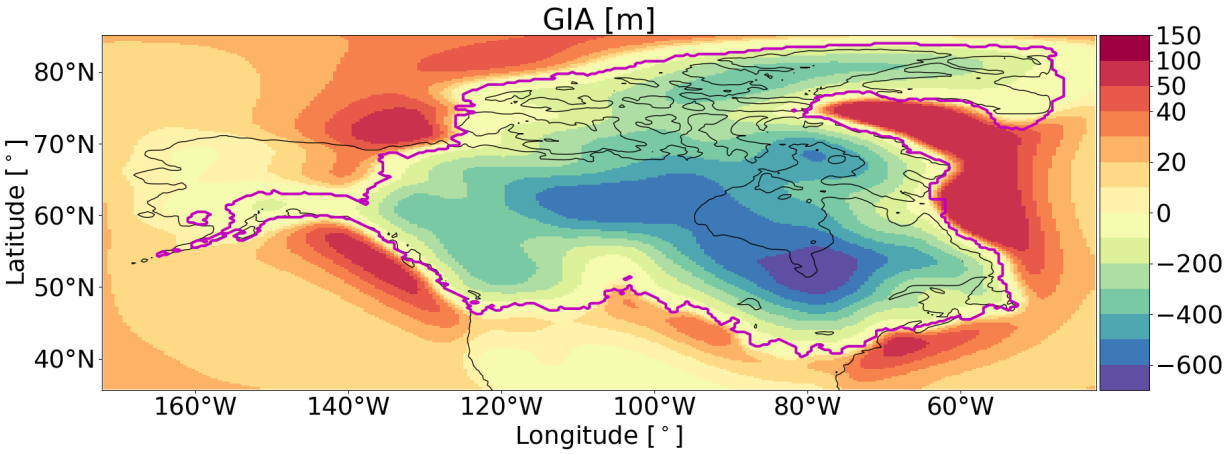

Figure S36. GIA for parameter vector 5 at 20 kyr BP compared to the bed topography at 120 kyr BP. The magenta contour line represents the grounding line. The black contour is the present-day sea level (coastline) used in the GSM.

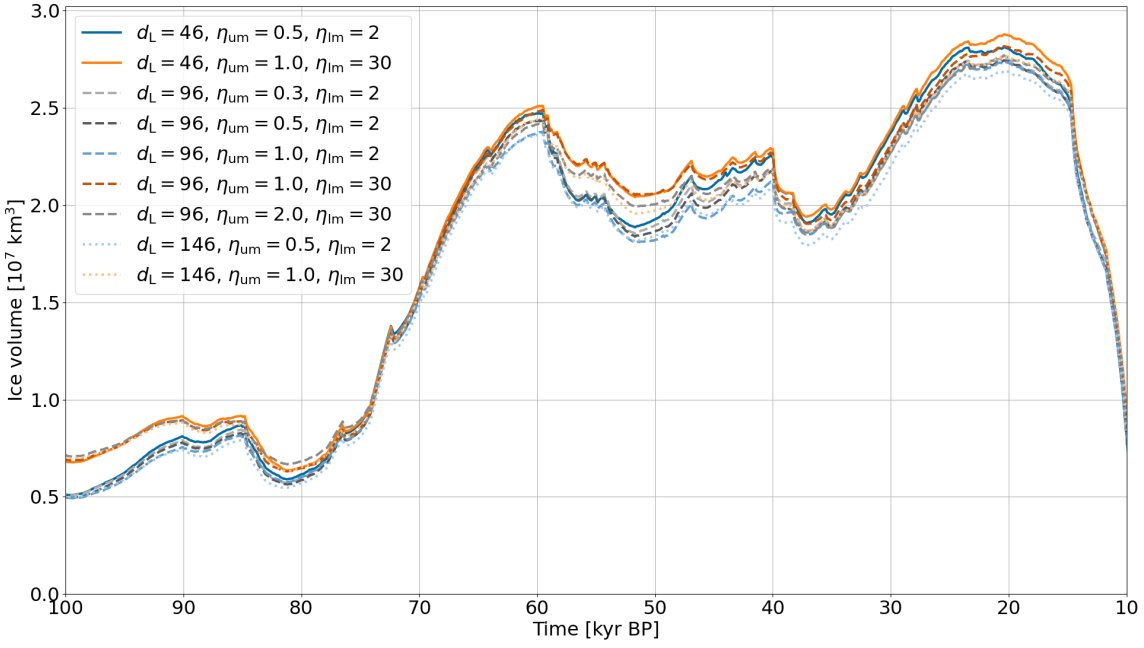

Figure S37. Mean North American ice volume across all 20 parameter vectors for 9 different earth rheology models of the global GIA model. d_L, η_{um}, and η_{lm} are the thickness of the Lithosphere (km), the viscosity of the upper mantle and the viscosity of the lower mantle (10^{21} Pa s), respectively.

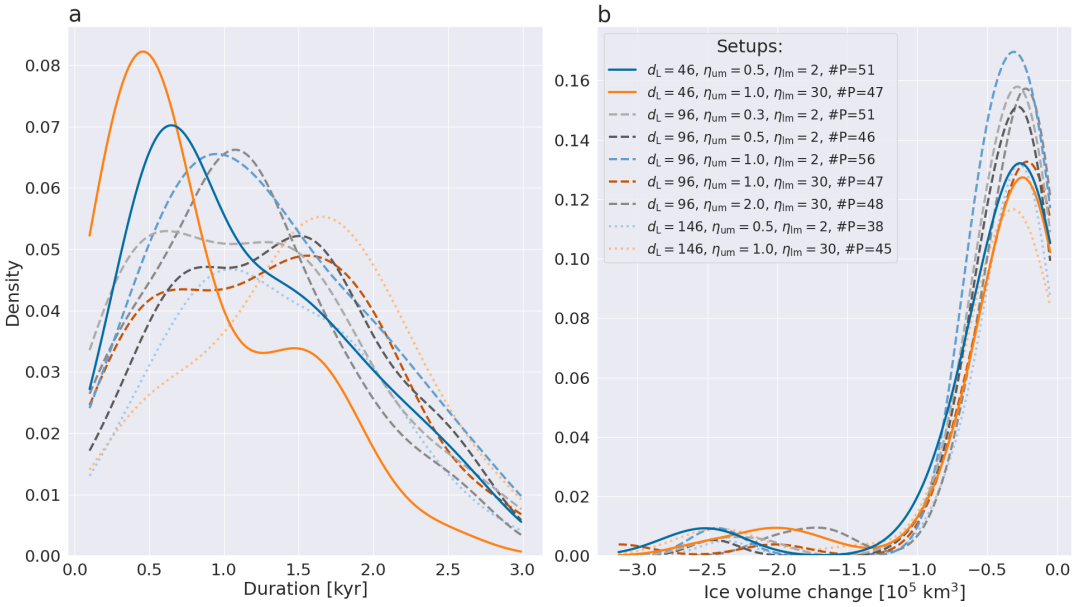

Figure S38. Kernel density plot for different earth rheologies (whole ensemble) when using the global GIA model. Each line is based on the surges within all runs with the same earth rheology model. d_{L}, η_{um}, and η_{lm} are the thickness of the Lithosphere (km), the viscosity of the upper mantle and the viscosity of the lower mantle (10^{21} Pa s), respectively. #P indicates the total number of surges across all runs of the ensemble.

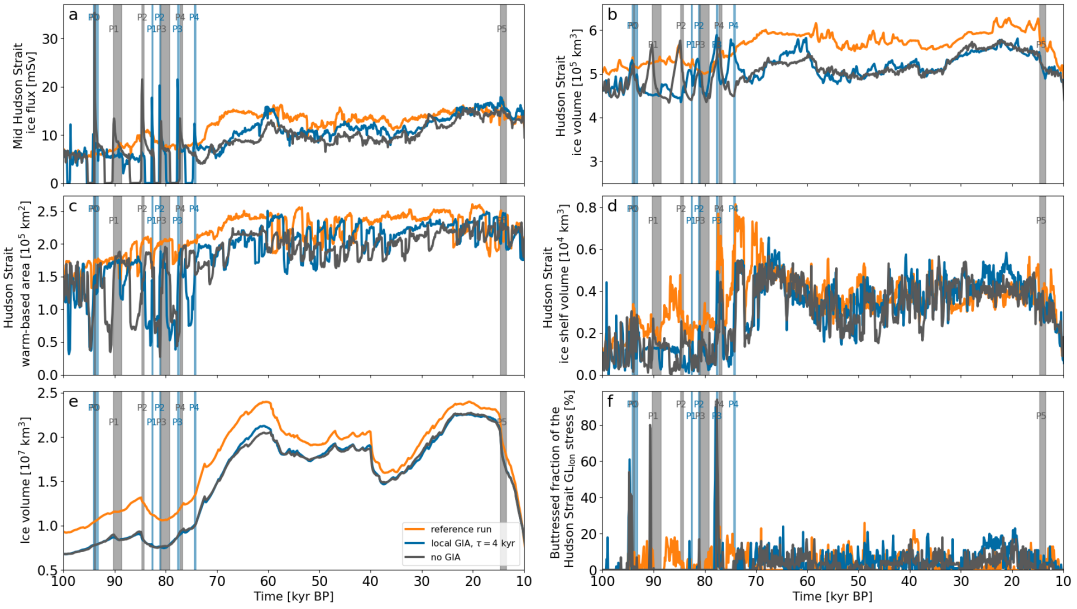

Figure S39. Time series of parameter vector 16 when using different GIA models. Panel e shows the overall North American ice volume. Otherwise as Fig. 4.

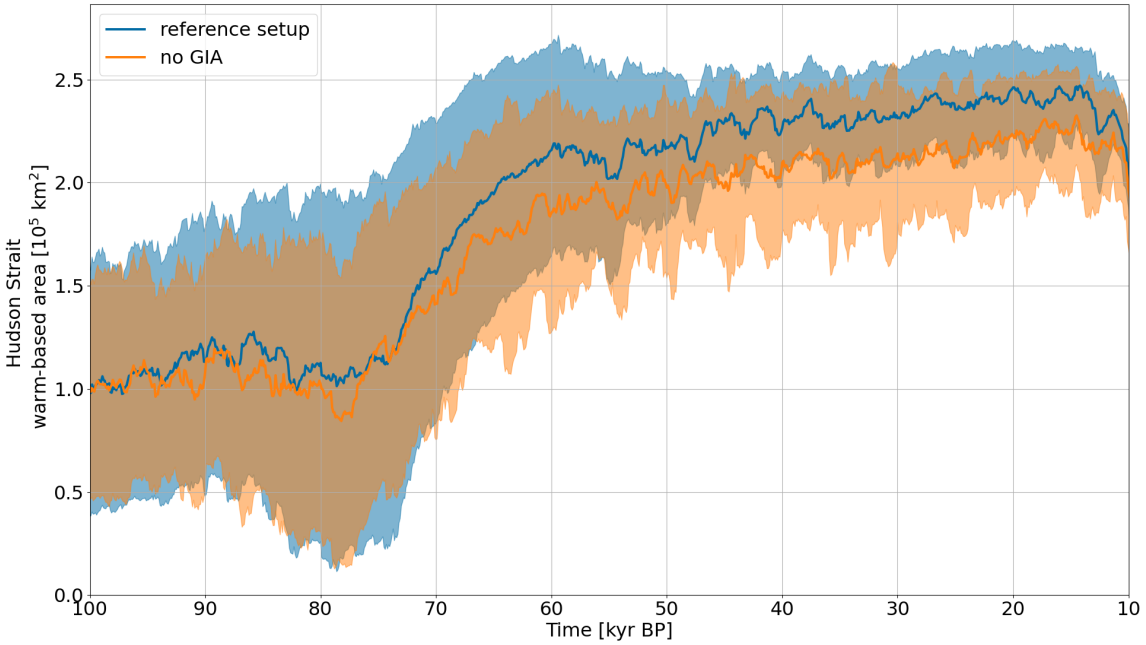

Figure S40. Hudson Strait warm-based area for the reference setup (global GIA model) and runs without GIA. The thick lines and shaded areas represent the mean and mean±standard deviation of 18 runs, respectively (the runs for parameter vectors 8 and 15 crashed in the comparison setup and were not included).

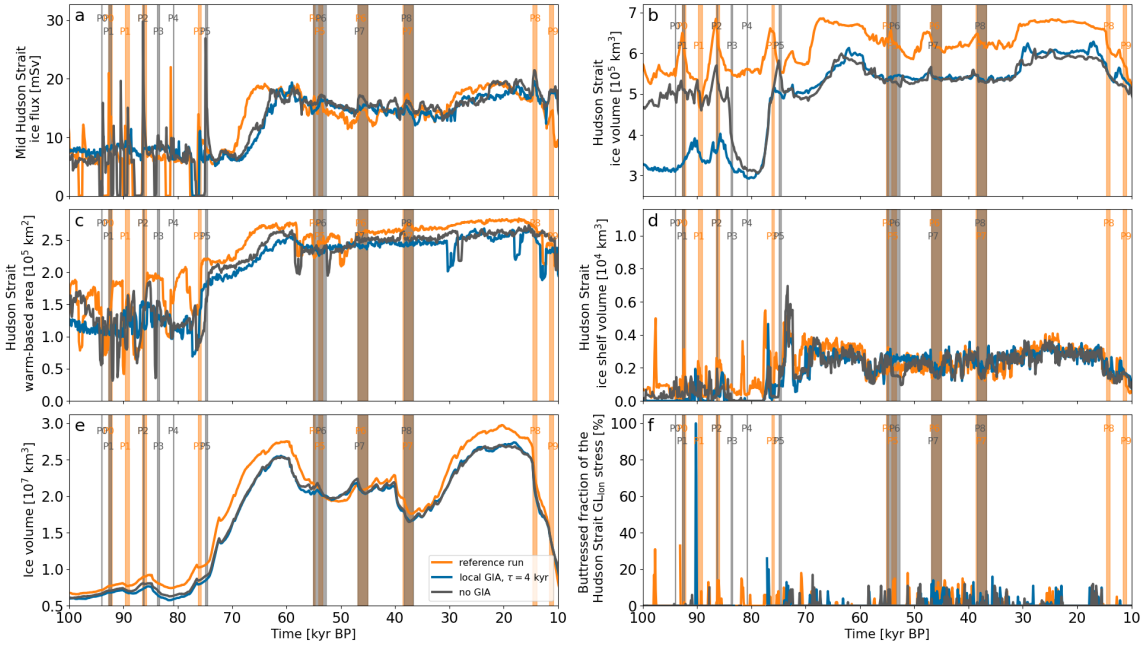

Figure S41. Time series of parameter vector 11 when using different GIA models. Panel e shows the overall North American ice volume. Otherwise as Fig. 4.

45 S10 Geothermal heat flux

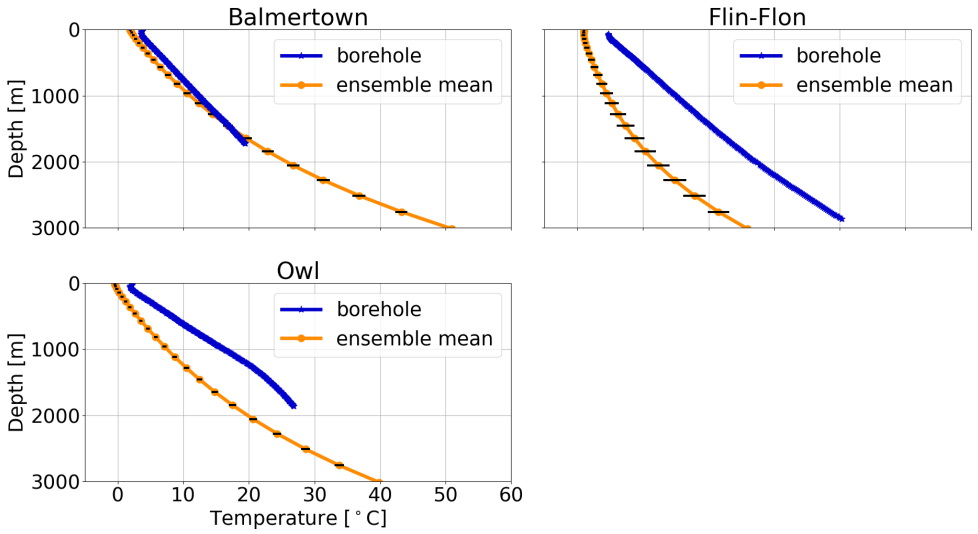

Figure S42. Bed temperature profiles for the Balmertown (93.7167°W, 51.0333°N, Rolandone et al., 2003), Flin-Flon (102.0°W, 54.717°N, J. C. Mareschal, personal communication, 2006), and Owl (97.86°W, 55.67°N, Rolandone et al., 2002) boreholes and the corresponding GSM grid cells. The location of the boreholes is shown in Fig. S43. The orange lines and black horizontal bars represent the present-day ensemble mean and standard deviation of the GSM reference setup (default GHF (Fig. 1a), Davies, 2013), respectively.

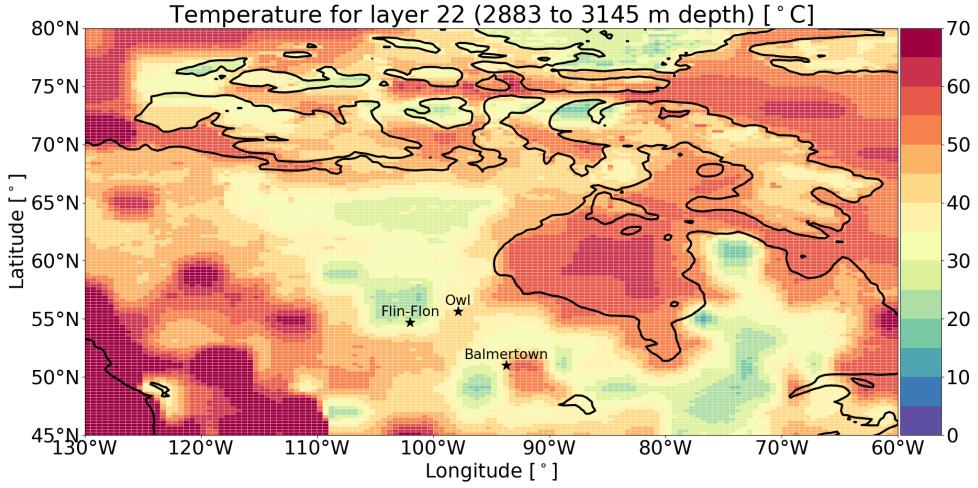

Figure S43. Bed temperature field between 2883 and 3145 m depth in the GSM. The default GHF (Fig. 1a) was used (Davies, 2013). The black asterisks mark the locations of the boreholes shown in Fig. S42. The black contour line shows the present-day sea level (coastline) used in the GSM.

S11 Labrador ice shelf volume

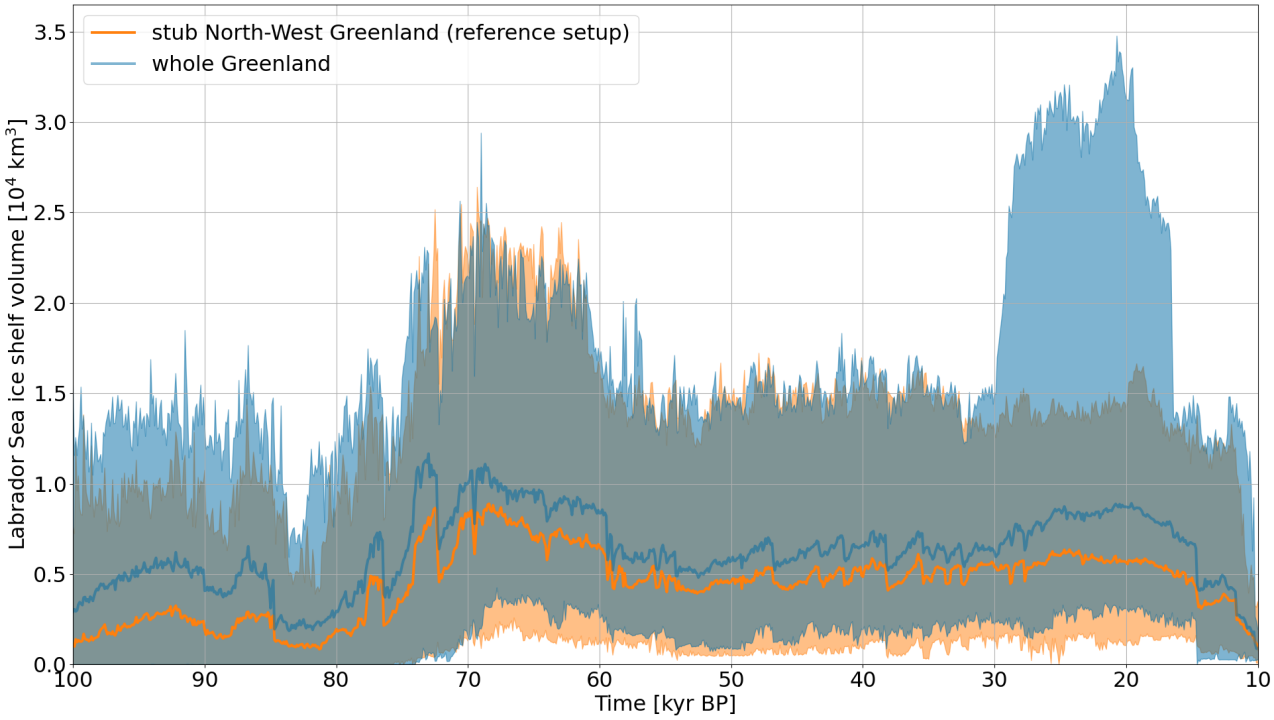

Figure S44. Labrador Sea ice shelf volume in the *Labrador Sea ice shelf area* outlined in Fig. 2 for a stub North-West Greenland (reference setup) and whole Greenland. The thick lines represent the mean of the 20 run ensembles. The shaded area mark the minimum and maximum of the ensembles. The whole Greenland runs for parameter vectors 8 and 15 crashed are not considered here.

References

Bassis, J. N., Petersen, S. V., and Mac Cathles, L.: Heinrich events triggered by ocean forcing and modulated by isostatic adjustment, Nature, 542, 332—334, https://doi.org/10.1038/nature21069, 2017.

Bazin, L., Landais, A., Lemieux-Dudon, B., Toyé Mahamadou Kele, H., Veres, D., Parrenin, F., Martinerie, P., Ritz, C., Capron, E., Lipenkov, V., Loutre, M.-F., Raynaud, D., Vinther, B., Svensson, A., Rasmussen, S. O., Severi, M., Blunier, T., Leuenberger, M., Fischer, H., Masson-Delmotte, V., Chappellaz, J., and Wolff, E.: An optimized multi-proxy, multi-site Antarctic ice and gas orbital chronology (AICC2012): 120 - 800 ka, Climate of the Past, 9, 1715–1731, https://doi.org/10.5194/cp-9-1715-2013, 2013.

Blackwell, D. and Richards, M.: Geothermal Map of North America, AAPG Map, scale 1:6,500,000, Product Code 423, https://www.smu.edu/-/media/Site/Dedman/Academics/Programs/Geothermal-Lab/Graphics/Geothermal_MapNA_7x10in.gif, last accessed: 2024-11-07, 2004.

Bradley, R.: PALEOCLIMATOLOGY (3rd edition), Academic Press, 2014.

Davies, J. H.: Global map of solid Earth surface heat flow, Geochemistry, Geophysics, Geosystems, 14, 4608–4622, https://doi.org/10.1002/ggge.20271, 2013.

Gibb, O. T., Hillaire-Marcel, C., and de Vernal, A.: Oceanographic regimes in the northwest Labrador Sea since Marine Isotope Stage 3 based on dinocyst and stable isotope proxy records, Quaternary Science Reviews, 92, 269–279, https://doi.org/10.1016/j.quascirev.2013.12.010, 2014.

Pollack, H. N., Hurter, S. J., and Johnson, J. R.: Heat flow from the Earth's interior: Analysis of the global data set, Reviews of Geophysics, 31, 267–280, https://doi.org/https://doi.org/10.1029/93RG01249, 1993.

Pollard, D. and Deconto, R. M.: Improvements in one-dimensional grounding-line parameterizations in an ice-sheet model with lateral variations (PSUICE3D v2.1), Geoscientific Model Development, 13, 6481–6500, https://doi.org/10.5194/gmd-13-6481-2020, 2020.

Rasmussen, T. L. and Thomsen, E.: The role of the North Atlantic Drift in the millennial timescale glacial climate fluctuations, Palaeogeography, Palaeoclimatology, Palaeoecology, 210, 101–116, https://doi.org/10.1016/j.palaeo.2004.04.005, 2004.

Rolandone, F., Jaupart, C., Mareschal, J. C., Gariépy, C., Bienfait, G., Carbonne, C., and Lapointe, R.: Surface heat flow, crustal temperatures and mantle heat flow in the Proterozoic Trans-Hudson Orogen, Canadian Shield, Journal of Geophysical Research: Solid Earth, 107, ETG 7–1–ETG 7–19, https://doi.org/10.1029/2001jb000698, 2002.

Rolandone, F., Mareschal, J. C., and Jaupart, C.: Temperatures at the base of the Laurentide Ice Sheet inferred from borehole temperature data, Geophysical Research Letters, 30, 18–21, https://doi.org/10.1029/2003GL018046, 2003.

Schoof, C.: Marine ice-sheet dynamics. Part 1. The case of rapid sliding, Journal of Fluid Mechanics, 573, 27–55, https://doi.org/10.1017/S0022112006003570, 2007.

Tarasov, L. and Goldstein, M.: Assessing uncertainty in past ice and climate evolution: overview, stepping-stones, and challenges, EGUsphere [preprint], 2021, 1–54, https://doi.org/10.5194/cp-2021-145, 2021.

Tarasov, L., Lecavalier, B. S., Hank, K., and Pollard, D.: The glacial systems model (GSM), https://www.physics.mun.ca/~lev/GSM.pdf, last accessed: 2024-11-07, 2024.

Veres, D., Bazin, L., Landais, A., Toyé Mahamadou Kele, H., Lemieux-Dudon, B., Parrenin, F., Martinerie, P., Blayo, E., Blunier, T., Capron, E., Chappellaz, J., Rasmussen, S. O., Severi, M., Svensson, A., Vinther, B., and Wolff, E. W.: The Antarctic ice core chronology (AICC2012): an optimized multi-parameter and multi-site dating approach for the last 120 thousand years, Climate of the Past, 9, 1733–1748, https://doi.org/10.5194/cp-9-1733-2013, 2013.